Report

Cell Reports

Ire1 Has Distinct Catalytic Mechanisms for *XBP1/HAC1* Splicing and RIDD

Graphical Abstract

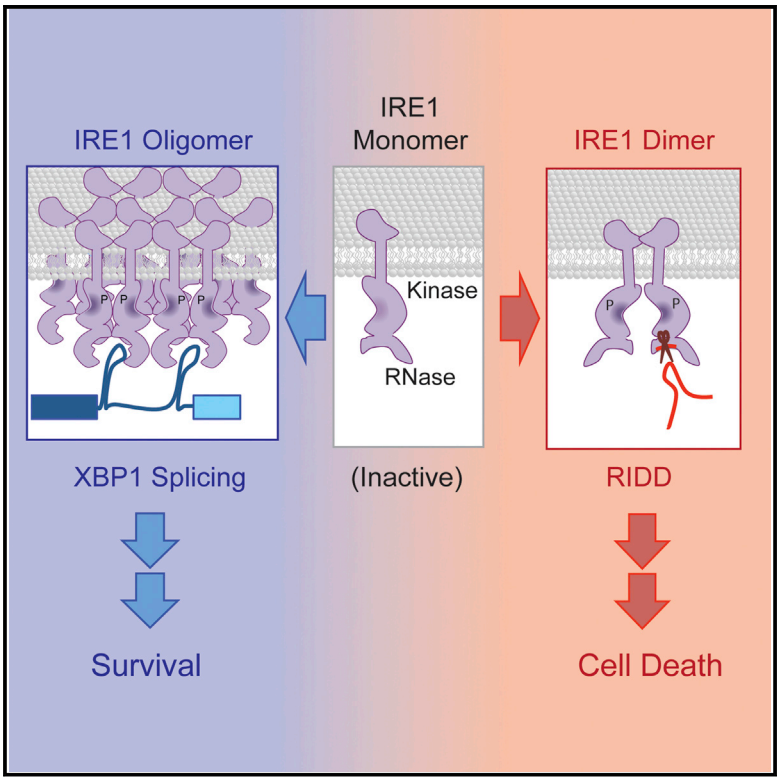

Highlights

Cleavage of *XBP1/HAC1* intron by IRE1 is a distinct and separable activity from RIDD

Oligomerization of active IRE1 is required for *XBP1/HAC1* cleavage but not RIDD

Both activities use the same catalytic residues but different substrate binding sites

Selective activation of RIDD promotes cell death, whereas *XBP1/HAC1* splicing supports survival

Authors

Arvin B. Tam, Albert C. Koong, Maho Niwa

Correspondence

niwa@ucsd.edu

In Brief

IRE1, an endoplasmic reticulum (ER) kinase/RNase, splices *XBP1/HAC1* to produce an active transcription factor but also cleaves ER-associated mRNA through regulated IRE1-dependent decay (RIDD). Using biochemical studies, Tam et al. demonstrate that cleavage of *XBP1* and *HAC1* and RIDD are distinct and separable activities. Cooperative action of IRE1 subunits within the oligomer is required for maximum *XBP1/HAC1* splicing activity. In contrast, RIDD does not require such cooperativity or oligomer formation. Additionally, selective activation of RIDD results in cell death.

Tam et al., 2014, Cell Reports 9, 850–858
November 6, 2014 ©2014 The Authors
http://dx.doi.org/10.1016/j.celrep.2014.09.016

OPEN ACCESS
CellPress

Cell Reports
Report

Ire1 Has Distinct Catalytic Mechanisms for *XBP1/HAC1* Splicing and RIDD

Arvin B. Tam,[1] Albert C. Koong,[2] and Maho Niwa[1,*]
[1]Division of Biological Sciences, Section of Molecular Biology, UCSD, La Jolla, CA 92093-0377, USA
[2]Department of Radiation Oncology, Stanford School of Medicine, Stanford, CA 94305-5152, USA
*Correspondence: niwa@ucsd.edu
http://dx.doi.org/10.1016/j.celrep.2014.09.016

SUMMARY

An evolutionarily conserved unfolded protein response (UPR) component, IRE1, cleaves *XBP1/HAC1* introns in order to generate spliced mRNAs that are translated into potent transcription factors. IRE1 also cleaves endoplasmic-reticulum-associated RNAs leading to their decay, an activity termed regulated IRE1-dependent decay (RIDD); however, the mechanism by which IRE1 differentiates intron cleavage from RIDD is not well understood. Using in vitro experiments, we found that IRE1 has two different modes of action: *XBP1/HAC1* is cleaved by IRE1 subunits acting cooperatively within IRE1 oligomers, whereas a single subunit of IRE1 performs RIDD without cooperativity. Furthermore, these distinct activities can be separated by complementation of catalytically inactive IRE1 RNase and mutations at oligomerization interfaces. Using an IRE1 RNase inhibitor, STF-083010, selective inhibition of *XBP1* splicing indicates that *XBP1* promotes cell survival, whereas RIDD leads to cell death, revealing modulation of IRE1 activities as a drug-development strategy.

INTRODUCTION AND RESULTS

IRE1 is a transmembrane receptor kinase located on the surface of the endoplasmic reticulum (ER) that initiates the unfolded protein response (UPR) pathway and is required for the ER to function properly. Upon activation, IRE1 becomes an active endoribonuclease (RNase) that cleaves an intron of an mRNA coding for a bZIP transcription factor, *HAC1* in yeast or *XBP1* in mammalian cells (Calfon et al., 2002; Gonzalez et al., 1999; Kawahara et al., 1997; Sidrauski and Walter, 1997). Cleaved exons are then ligated by tRNA ligase in the case of *HAC1* (Sidrauski et al., 1996) and RtcB for *XBP1* (Lu et al., 2014) generating the spliced form of *HAC1* or *XBP1* mRNA. The IRE1-dependent splicing step is critical for mounting the UPR, as only the spliced form of *HAC1* or *XBP1* mRNA produces a potent transcription factor that induces UPR gene expression needed for re-establishment of ER functions.

Recently, UPR-activated IRE1 in several organisms—including *S. pombe*, mammalian, *Drosophila*, and plant cells—has been reported to also cleave a subset of mRNA that is associated with the ER membrane (Han et al., 2009; Hollien et al., 2009; Hollien and Weissman, 2006; Kimmig et al., 2012; Mishiba et al., 2013) In these cases, however, IRE1-mediated cleavage is followed by degradation, a process that has been termed regulated IRE1-dependent decay (RIDD) (Hollien et al., 2009). At present, a detailed, mechanistic understanding of IRE1 engaged in either RIDD or *XBP1* mRNA intron cleavage is lacking. IRE1 that cleaves the *XBP1* intron must be coordinated with a ligase to generate the spliced form of *XBP1*. In contrast, IRE1 engaged in RIDD must be coupled with mRNA degradation enzymes in order to prevent either translating or ligating cleavage products. Curiously, RIDD has never been reported to occur in the budding yeast, *S. cerevisiae*.

To investigate the mechanistic relationship between *XBP1/HAC1* splicing and RIDD, we first asked if IRE1 from the budding yeast *S. cerevisiae* can perform RIDD cleavage events. After treating cells with tunicamycin (Tm), a well-characterized inducer of UPR, levels of two mRNAs, *DAP2* (*DPAPB*) and *MFα1* (*α-Factor*) coding for secretory pathway proteins (Figure S1A), decreased in agreement with genome-wide transcription analyses (Gasch et al., 2000; Travers et al., 2000). The decrease in mRNA levels required IRE1 but not *HAC1* (Figure S1A) and was well correlated with the kinetics of *HAC1* splicing (Figure S1B). Using an in vitro RNase assay, recombinant yeast IRE1 (yIre1) can cleave *HAC1* RNA (Figure S1C) and in vitro transcribed radiolabeled *DAP2* (Figure 1A) and *MFα1* (Figure S1D) RNA upon incubation with ADP. The RNA cleavage fragments generated by yIre1 cleaving mammalian mRNAs that are known substrates for RIDD such as *BLOS1* or *INSULIN* were essentially identical to those generated by human recombinant IRE1 (hIre1) (compare Figures 1A and 1B). Notably, recombinant yeast and human Ire1 did not cleave the mRNA of *ACTIN*, a nonsecretory protein, demonstrating that Ire1 is not a random nonspecific RNase (Figure S1C). Furthermore, mutating the invariant guanosine (Gonzalez et al., 1999; Han et al., 2009; Kawahara et al., 1997) located at the RIDD cleavage site of the *INSULIN* mRNA abolished cleavage at that site and instead generated aberrantly cleaved fragments (Figure S1E), reminiscent of other RNA processing events (Yang, 2011). These results demonstrate that RIDD activity is conserved in yIre1.

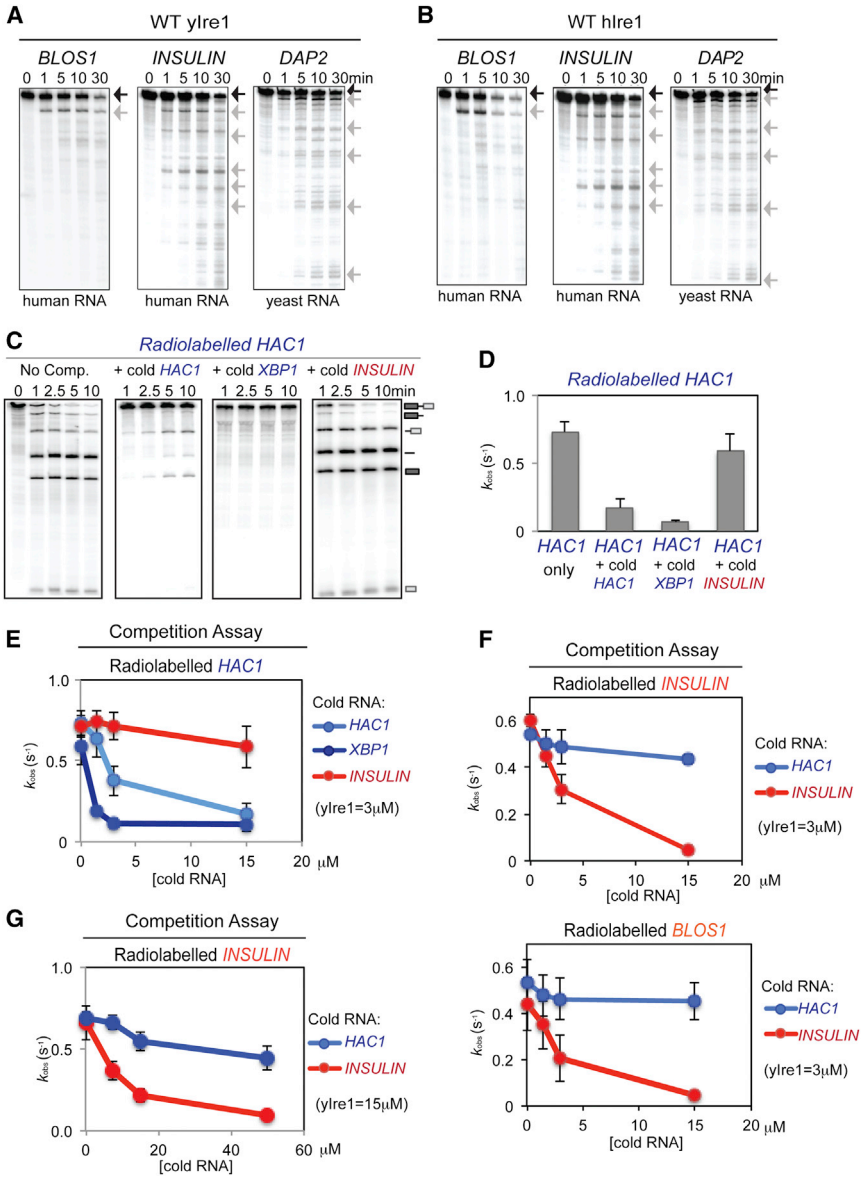

Figure 1. In Vitro Cleavage of RIDD Substrate RNA Is Distinct from *XBP1/HAC1* Cleavage

(A and B) In vitro cleavage of RIDD. In vitro transcribed radiolabeled mammalian (*BLOS1*, *INSULIN*) and yeast (*DAP2*) RNA substrates (0.5 nM) were incubated with ADP (2 mM) and 1 μM recombinant WT yIre1 (A) or WT hIre1 (B) for up to 30 min. Black arrow, full-length RNA; gray arrow, cleaved RNA fragments.

(C and D) Using single-turnover conditions (Figure S1F), *HAC1* RNA cleavage reactions were competed by excess unlabeled (cold) *HAC1* or *XBP1* RNA (15 μM) but not with RIDD RNA (15 μM). Reactions were performed with 2 mM ADP for up to 10 min. (C) k_{obs} calculated from these reactions are shown in (D). Error bars of all the experiments in this figure represent at least three independent repeats.

(E) *HAC1* RNA cleavage reactions with different concentrations of various competitor RNAs (representative reactions shown Figures S1G and S1H).

(F) RIDD reactions are competed by RIDD substrate RNA but not by *HAC1* RNA (representative reactions shown in Figures S1K and S1L).

(G) RIDD RNA cleavage competition reactions performed under single turnover conditions (Figure S2A) (representative reactions shown in Figure S2B).

XBP1/HAC1 RNA Cleavage Is Not Competed by RIDD Substrates

To determine the molecular relationship between IRE1-mediated cleavage of *HAC1* and RIDD substrate RNAs, we performed in vitro yIre1 RNase reactions with radiolabeled RNA substrates in the presence of unlabeled (cold) RNA competitors. If IRE1 uses the same active site for binding and cleavage of both *HAC1* and RIDD substrates, then *both* substrate RNAs should compete for the same active site. However, if the active sites are different, then *HAC1* and RIDD RNA substrates should not compete equally well under single turnover conditions (Figure S1F). Cleavage of radiolabeled *HAC1* RNA decreased upon addition of increasing amounts of cold *HAC1* RNA, resulting in the accumulation of uncleaved radiolabeled *HAC1* RNA (Figures 1C–1E and S1G). The addition of cold *XBP1* RNA also resulted in decreased cleavage of radiolabeled *HAC1* RNA (Figures 1C–1E, and S1H). Conversely, cold *HAC1* also inhibited cleavage of radiolabeled *XBP1* (Figures S1I and S1J). In contrast, addition of cold *INSULIN* RNA at a high concentration (15 μM) did not notably affect the cleavage of radiolabeled *HAC1* RNA (Figures 1C–1E and S1G). The converse was also true: cleavage of radiolabeled *INSULIN* RNA was inhibited by excess amounts of cold *INSULIN* RNA but not *HAC1* RNA (Figures 1F and S1K). Furthermore, the cleavage of another RIDD substrate, *BLOS1* RNA, was also inhibited by excess amounts of cold *INSULIN* RNA (Figures 1F and S1L). During these competition experiments, we noted that overall RIDD cleavage (either with *INSULIN* or *BLOS1* RNA) was rather less effective than *HAC1* or *XBP1* RNA cleavage, suggesting that 3 μM yIre1 might not truly represent a single turnover condition for RIDD cleavage. In fact, further experiments revealed that RIDD reaction was saturated at ~10 μM (Figure S2A). Thus, we performed a similar set of RIDD competition at yIre1 concentrations (15 μM) and found essentially the same results: cold *INSULIN* but not *HAC* RNA competed with *INSULIN* cleavage (Figures 1G and S2B). Taken altogether, these results suggest that Ire1 cleaves *HAC1* or RIDD RNA substrates using two distinctive binding and/or catalytic sites.

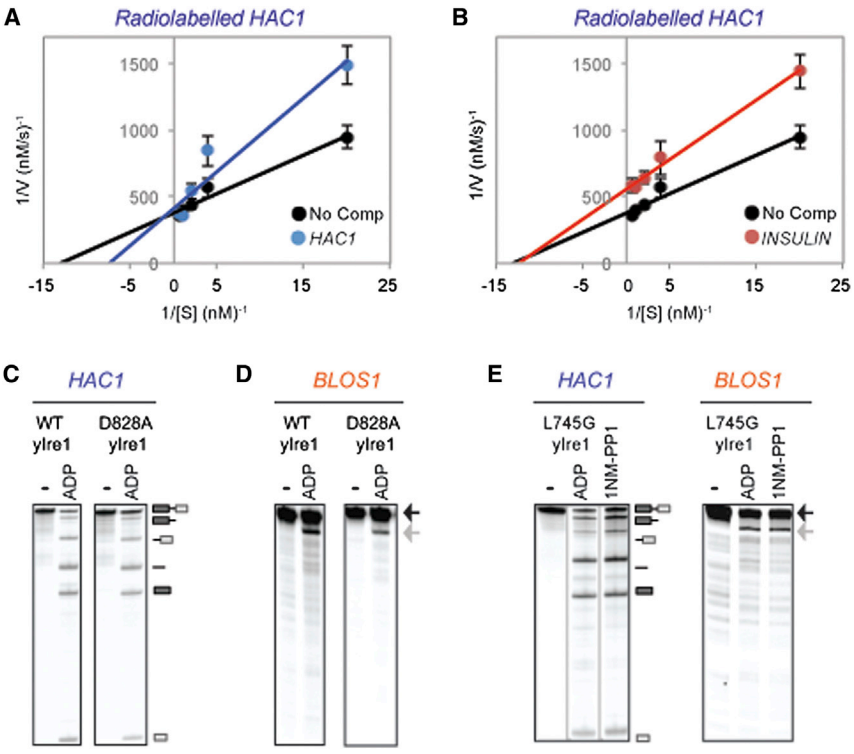

Figure 2. RIDD Requires the Nucleotide Binding in the IRE1 Kinase Domain and Exhibits Noncompetitive Inhibition with the *HAC1* RNA Cleavage Reaction

(A and B) Lineweaver-Burk plots of steady-state ylre1 RNase reactions cleaving radiolabeled *HAC1* containing no competitor (black), cold *HAC1* (blue) (A), or *INSULIN* RNA (red) (B). Error bars represent three independent repeats (representative reactions shown in Figure S2E).

(C and D) RNA cleavage reactions of *HAC1* (C) or *BLOS1* (D) RNA were performed with WT ylre1 or D828A ylre1 (1 μM) for 15 min. RNA cleavage fragments are indicated schematically.

(E) L745G ylre1 (1 μM) cleaves *BLOS1* and *HAC1* RNA in the presence of ADP or the nonhydrolyzable ATP homolog 1NM-PP1 (20 μM).

To determine whether these two forms can interchange, we performed competition assays under steady-state conditions using a decreased amount of protein (0.1 μM). The addition of 0.15, 0.3, and 1.5 μM cold *HAC1* RNA to radiolabeled *HAC1* RNA resulted in dose-dependent inhibition (Figure S2C). In Lineweaver-Burk plot, we found that inhibition of radiolabeled *HAC1* cleavage by cold *HAC1* RNA showed competitive inhibition (Figures 2A and S2E). In contrast, we found that cold *INSULIN* inhibited the cleavage of radiolabeled *HAC1* RNA (Figure S2D) in the mode of noncompetitive inhibition (Figures 2B and S2E), providing additional support that Ire1 has two distinct RNA substrate binding and/or catalytic sites for cleaving *HAC1* or RIDD RNA substrates.

IRE1 Kinase Domain Requirements for RIDD

Results of competition experiments were unexpected and raised a question of what conferred the mechanistic differences of Ire1 cleaving *XBP1/HAC1* or RIDD RNAs. Nucleotide binding is known to play a key role in activating Ire1 RNase for *XBP1/HAC1* RNA cleavage (Lee et al., 2008). D828 in ylre1 is important for coordinating magnesium (Mg^{2+}) in the active site, and a D828A ylre1 mutant is still able to bind ATP but is unable to transfer phosphates (Chawla et al., 2011). In agreement with previous work, WT and D828A ylre1 were able to cleave *HAC1* RNA (Figure 2C) (Chawla et al., 2011). Similarly, we found that WT and D828A ylre1 were also able to cleave *BLOS1* RNA (Figure 2D). The importance of nucleotide binding for both *HAC1* and RIDD RNA cleavage was further confirmed by the use of the L745G mutant ylre1, which has an altered nucleotide binding pocket capable of binding the nonhydrolyzable ATP homolog 1NM-PP1 (Papa et al., 2003). Upon binding to 1NM-PP1, L745G ylre1 was capable of cleaving both *HAC1* and *BLOS1* RNA (Figure 2E), indicating that binding in the nucleotide pocket is sufficient for RIDD activation. Taken altogether, the importance of the nucleotide binding in the Ire1 kinase domain is the same for cleavage of both *HAC1* and RIDD RNA and thus is unlikely to be the key determinant that differentiates *HAC1* and RIDD substrate cleavage.

Differences in IRE1 Cooperativity Distinguish between *XBP1/HAC1* and RIDD Substrate *RNA* Cleavage

The kinase domain of Ire1 is necessary for oligomer formation, an important step leading to *XBP1/HAC1* splicing, and the oligomer of Ire1 can be monitored by foci formation using IRE1-GFP (Aragón et al., 2009; Ishiwata-Kimata et al., 2013; Korennykh et al., 2009; Li et al., 2010). At 1 hr after treating HEK293 cells with thapsigargin (Tg), a well-characterized UPR-activating drug that disrupts calcium levels in the ER, the IRE1-GFP foci were detected (Figure S3A). These foci became larger at 4 hr and then had dispersed by 8 hr (Figure S3A). Samples collected at the same time showed *XBP1* splicing detectable within 1 hr of treatment and continuing for 4 hr before starting to decline (Figure S3B) as reported previously (Li et al., 2010). In contrast, significant levels of RIDD activity, which was calculated as a percentage of substrates cleaved (*BLOS1* and *SCARA3*), did not appear until 2 hr after UPR induction and continued to increase throughout the time course (Figure S3B). At the 8 hr time point, RIDD activity was at its highest, and no IRE1-GFP foci were present (Figures S3A and S3B). Our finding in vitro that both *XBP1* and RIDD substrate RNA cleavage occurred within a minute of incubation revealed that IRE1 was capable of cleaving either substrate with similar kinetics (Figures 1A, 1B, and S1C). The differences observed here in vivo might come from differential availabilities of these RNA substrates. However, both *XBP1* and *BLOS1* mRNA were associated with the ER membrane even prior to

ER stress induction (Figure S3C). This suggests that a regulatory step(s) beyond RNA localization is unlikely to be responsible for generating the differences in activation kinetics of *XBP1* splicing and RIDD in vivo. Although factors other than the RNA cleavage by IRE1, including the ligation step for *XBP1* splicing or degradation of the cleaved fragments for RIDD, affect the appearance of the spliced form of *XBP1* or overall levels of RIDD substrate mRNA in cells, these findings hinted that formation of IRE1 higher ordered structures, which correlate with *XBP1* mRNA splicing, might not be necessary for RIDD activity, and warranted for further examination.

To investigate contributions of higher order structure of Ire1 in the *XBP1* or RIDD RNA cleavage, we tested cooperativity of Ire1 and determined the Hill coefficient to be 2.13 ± 0.38 for yIre1-cleaving *HAC1* RNA (Figures 3A and S3D) and similarly the Hill coefficient for hIre1 cleaving *XBP1* RNA to be 3.07 ± 0.65 (Figures 3A and S3E), indicating that Ire1 RNase for *HAC1* or *XBP1* consists of Ire1 complex with the presence of cooperativity (Korennykh et al., 2009). In contrast, the Hill coefficients for the RIDD reactions were 1.15 ± 0.19 for yIre1 and 1.10 ± 0.29 for hIre1, indicating essentially no cooperativity (Figures 3A, S3D, and S3E). In addition, we found that the Hill coefficient value for a *HAC1* substrate with only one cleavage due to a mutation at the 3′ splice site (Figure S3F) was similar to that for the WT *HAC1 RNA*, revealing that the number of cleavage sites does not matter for cooperativity.

In addition to Hill coefficients, we also performed transcomplementation assays using WT and H1061N (a catalytically inactive mutant) yIre1. Previous studies found that H1061 participates in the proton relay mechanism necessary for cleaving *HAC1* RNA (Korennykh et al., 2011). A mutation at this site prevents cleavage of *HAC1* RNA without disrupting yIre1 oligomer formation (Figures S3G and S3H) (Korennykh et al., 2011). Furthermore, we found that H1061N yIre1 was also inactive for RIDD substrate cleavage (Figure S3G). In the transcomplementation assay, we kept the concentration of WT yIre1 constant at 0.083 μM where yIre1 remained as a monomer upon performing the previously reported oligomerization assay (Figure S3H) (Korennykh et al., 2011). Furthermore, WT yIre1 showed very little cleavage activity for either *HAC1* or RIDD substrates (Figure 3B, lanes 1 and 7). As increasing amounts of H1061N yIre1 were added, the heterocomplexes became active for *HAC1* cleavage (Figure 3B, lanes 2–5), consistent as previously reported (Korennykh et al., 2011). However, once the concentration of H1061N yIre1 far exceeded that of WT yIre1, *HAC1* RNA cleavage became inactive (Figure 3B, lane 6). In contrast, RIDD RNA cleavage was restored when H1061N yIre1 was added at an equal or 2-fold higher concentration of WT yIre1 (Figure 3B, lanes 7–9), but higher levels of H1061N yIre1 inhibited RIDD cleavage (Figure 3B, lanes 10–12).

Oligomerization State of IRE1 Can Distinguish between *HAC1* and RIDD Substrate *RNA* Cleavage

These observations also provided a prediction that disruption of the interfaces within the yeast Ire1 oligomers has little impact on RIDD cleavage. To test this idea, we prepared three mutant forms of yeast Ire1 carrying a mutation at one of the three interfaces: IF1^{c} Glu 988, IF2^{c} Arg 1087, and IF3^{c} Arg 899, generating E988Q, R1087D, and R899A yIre1, respectively (Korennykh et al., 2009) (Figure 3C). All three yIre1 interface mutants did not generate oligomers based on the oligomerization assay (Figure S3H) (Korennykh et al., 2009). In agreement with previous reports (Korennykh et al., 2009; Lee et al., 2008), we found that alterations in any of these residues inactivated *HAC1* RNA cleavage (Figure 3D). In contrast, IF2^{c}-R1087D yIre1 remained active for RIDD at the rate similar to WT yIre1 (Figures 3E and 3F), whereas E988Q and R899A yIre1 did not show RIDD cleavage (Figures 3D and 3E). R1087 is localized between the two RNase interface in the oligomer (Figure 3C), and the ability of R1087D yIre1 to retain the cleavage of RIDD RNA, but not that of *HAC1* RNA, provided a further support for the different nature of RIDD RNase reactions.

Curiously, we found that both E988Q yIre1 and R1087D yIre1 were active kinases able to undergo autophosphorylation (Figure S3I) (Chawla et al., 2011; Han et al., 2009; Lee et al., 2008). E988Q yIre1 is an inactive RNase for both *HAC1* RNA and RIDD, suggesting that activation of the kinase domain alone is not sufficient to generate an active Ire1 RNase. This is a notable result as the current model proposes that Ire1 initially forms ''face-to-face'' dimers where the nucleotide binding pockets are facing each other within Ire1 dimer (Figure S4A), and structural studies reveal that the two RNase domains are not in close proximity (Figure S4A) (Ali et al., 2011). Presumably, formation of dimers in a ''back-to-back'' form where the nucleotide binding pockets are facing away from each other brings two RNase domains together to create a catalytically active RNase (Lee et al., 2008). The back-to-back dimer is present in the crystalized oligomer that corresponds to the IF1^{c} interface (compare Figure S4A [back-to-back dimer] with Figure 3C [IF1^{c}]) (Korennykh et al., 2009). Recently, quercetin (Q) has been shown to induce the formation of yIre1 back-to-back dimers by binding to the Q site, an interface between the kinase and RNase domain (Figure S4A) (Wiseman et al., 2010). Q binding can occur independent of Ire1 kinase domain and activates Ire1 RNase for cleavage of *HAC1* RNA (Figures 4A and S4B) (Wiseman et al., 2010). Similarly, we found that the binding of Q to Ire1 was sufficient to promote cleavage of RIDD substrate RNA (Figures 4A and S4B). Given that RIDD does not require oligomer formation (Figures 3A and 3D–3F), these results suggest that the Ire1 back-to-back dimer itself is sufficient for RIDD cleavage.

To further understand the mechanistic differences in Ire1 for *HAC1* RNA and RIDD cleavage, we examined the effect of the Ire1 RNase specific inhibitor STF-083010 (STF) on yIre1 activated by ADP or Q. We found that *HAC1* cleavage by ADP- or Q-activated yIre1 was effectively inhibited by STF, both with an IC_{50} around 30 μM (Figure 4B) (Papandreou et al., 2011). STF also potently inhibited cleavage of RIDD substrates when yIre1 was activated by ADP (Figures 4B [orange closed circles] and 4D). In contrast, however, STF was not able to inhibit Q-induced RIDD as effectively as ADP activated RIDD even at higher concentration (Figure 4B [compare open with closed orange circles] and 4D). Structural comparisons of ADP-bound Ire1 (Figure 4C, in purple) (Korennykh et al., 2009) and Q-bound Ire1 (in green)

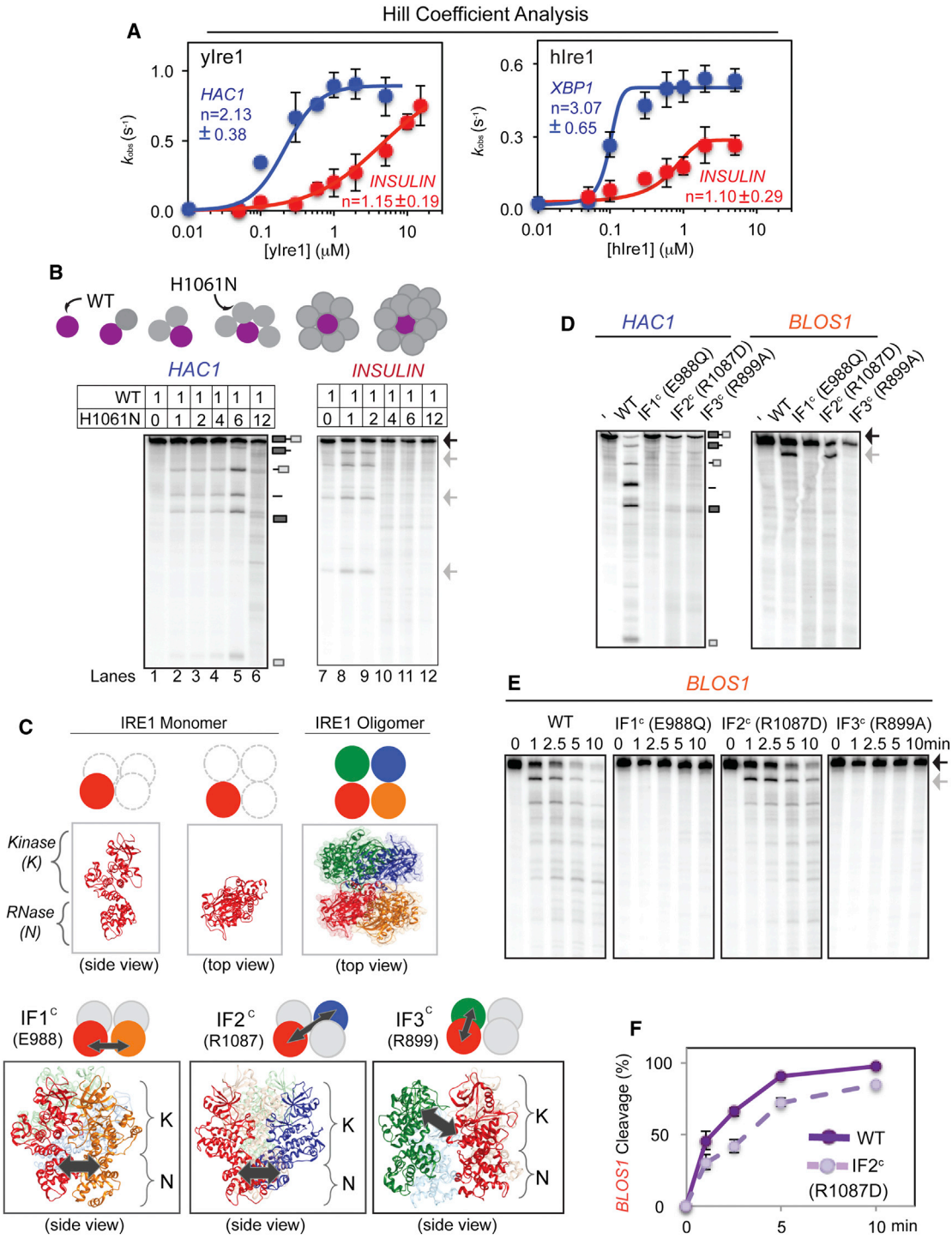

Figure 3. Cleavage of RIDD Substrate RNA Does Not Require Cooperative IRE1 Oligomerization

(A) Cooperative activation modes were observed for ylre1 and hIre1 cleaving *HAC1* and *XBP1* RNA, respectively, but not for cleaving *INSULIN* RNA. Cooperative Hill coefficients for ylre1/*HAC1* (2.13 ± 0.38) and hIre1/*XBP1* (3.07 ± 0.65) were found, while noncooperative values were found for ylre1/*INSULIN* (1.15 ± 0.19) and hIre1/*INSULIN* (1.10 ± 0.29). We interpret a noncooperative Hill coefficient of "1" as Ire1 acting as a dimer since unassociated, monomeric Ire1 is inactive (Lee et al., 2008), and the minimal active unit for Ire1 is a dimer (Figure S4A). All error bars in this figure were calculated from at least three independent experiments (representative reactions shown in Figures S3D and S3E).

(B) Transcomplementation assay between WT ylre1 and H1061N ylre1. WT ylre1 was kept at a concentration below the oligomerization threshold (0.083 μM) (Figure S3H) and inactive. Increasing amounts of catalytically inactive H1061N ylre1 at molar ratios from 1:0–1:12 ([WT]:[H1061N]) were added. A schematic of the experiment is shown in the top panel.

(legend continued on next page)

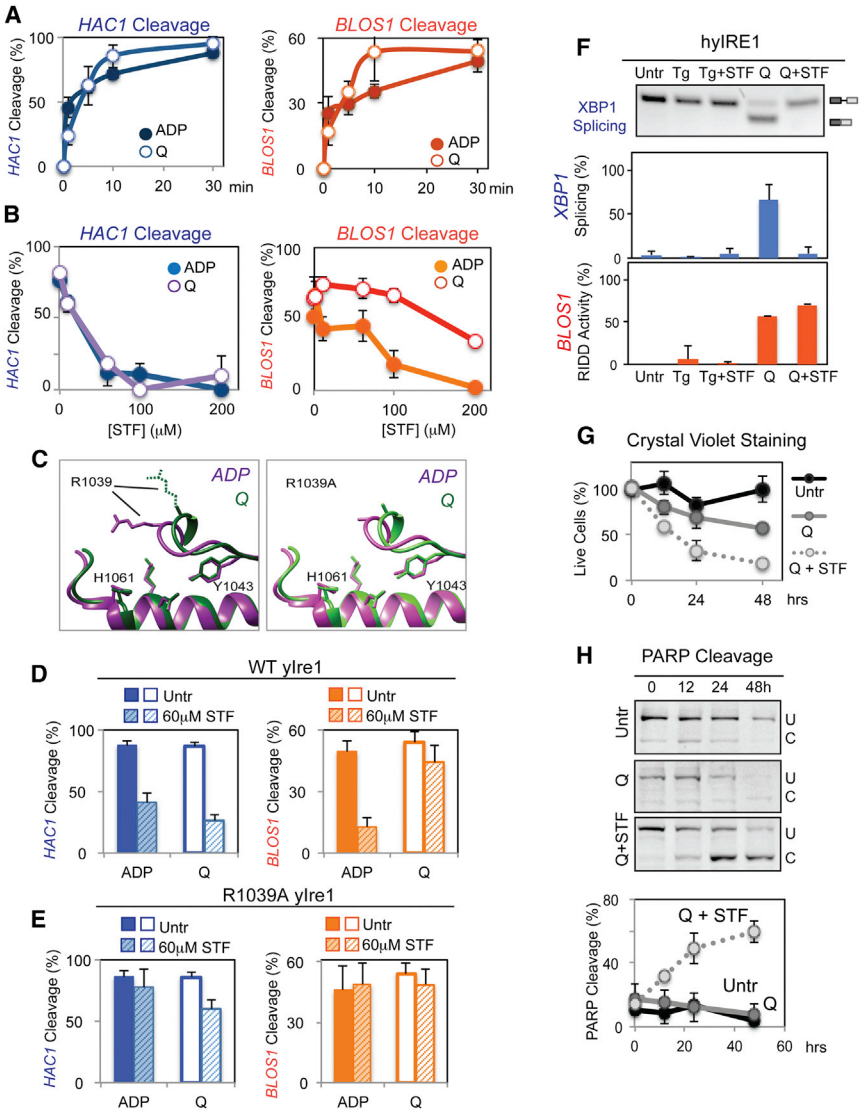

Figure 4. IRE1 RIDD Contributes to Cell Death

(A) Cleavage of *HAC1* (left) or *BLOS1* RNA (right) with WT yIre1 (1 μM) activated with ADP (2 mM) (closed circle) or Q (100 μM) (open circle). Error bars in this figure were calculated from at least three independent experiments.

(B) Nuclease reactions were performed with varying concentrations of STF-083010 (STF), an inhibitor, on WT yIre1 (1 μM) activated with either ADP (2 mM) (closed circles) or Q (100 μM) (open circles).

(C) The core RNase catalytic center between oligomerized Ire1, the ADP activated form "ADP" (purple) (Korennykh et al., 2009) and Q activated "Q" (green) yIre1 (Wiseman et al., 2010) is similar at the molecular level, except for the spatial orientation of the R1039 residue. The right panel shows structure predictions of R1039A yIre1 activated by ADP (purple) or Q (green).

(D and E) *HAC1* or RIDD cleavage by (D) WT yIre1 (1 μM) or (E) R1039A yIRE1 was activated by Q (100 μM) or ADP (2 mM) with and without STF (60 μM) for 30 min.

(F) STF inhibited *XBP1* mRNA splicing but not RIDD for Q-activated hybrid IRE1 (hyIRE1) in vivo with or without STF (60 μM) for 2 hr.

(G and H) Preferential inhibition of *XBP1* splicing but not RIDD in hyIRE1 induced (G) cell death and (H) apoptosis.

(Wiseman et al., 2010) revealed that the core catalytic residues, including H1061 and Y1043, remain unchanged but that the orientation of R1039 side chain became significantly different (Figure 4C, left). R1039 has been identified as a *HAC1* RNA binding residue (Korennykh et al., 2011). In fact, we found that altering R1039 to Ala in yIre1 diminished RNase activity for *HAC1* RNA as anticipated, but R1039A yIre1 remained active for the cleavage of *BLOS1* RNA similarly to WT yIre1 (Figure S4C), revealing that RIDD cleavage reaction does not engage R1039 residue as it does for *HAC1* RNA cleavage. Furthermore, R1039A yIre1 became insensitive to STF for the cleavage of both *HAC1* and *BLOS1* RNA (Figures 4E and S4D). Taken together, these observations suggest that R1039 residue of yIre1 is involved in *HAC1* RNA cleavage but does not play a significant role in the RIDD.

Differential Activation of IRE1 Determines Cell Fate Decisions

Preferential inhibition of Q-activated Ire1 cleavage of *HAC1* RNA but not RIDD substrates would provide a useful tool to dissect functional consequences of these two activities of Ire1. Q was not effectively taken up by yeast cells (Wiseman et al., 2010), which precluded the use of yeast for our analyses. Elegantly, a previous report demonstrated that a chimeric hybrid IRE1 (hyIRE1) where a human luminal domain was fused with the yeast cytosolic domain could be activated by Q when expressed in *ire1* knockout mouse embryonic fibroblasts (MEFs) (Wiseman et al., 2010). Using hyIRE1, we confirmed that hyIRE1 was not activated when Tg was used to induce ER stress, as reported previously (Figure 4F; Tg and Tg + STF). In contrast, incubation of hyIRE1 cells with Q activated hyIRE1 RNase for both *XBP1*

(C) Three interfaces in yIre1 oligomer (IF1^c E988, IF2^c R1087, and IF3^c R899) previously identified from X-ray crystallographic structure studies (Korennykh et al., 2009). One monomer of IRE1 (red) can contact three different monomers (orange, blue, green) within a tetramer, leading to the three interfaces, IF1^c, IF2^c, and IF3^c, respectively (bottom panel). Locations of IF1^c (E988), IF2^c (R1087), and IF3^c (R899) interactions are shown (arrows).

(D) Nuclease reactions were performed with either WT yIre1 or interface mutants IF1^c E988Q, IF2^c R1087D, and IF3^c R899A yIre1 (1 μM) for 10 min.

(E and F) Time course of *BLOS1* RNA cleavage reaction with WT yIre1 or yIre1 interface mutants (E) and the quantitation (F) of *BLOS1* RNA cleavage activities for WT and IF2^c yIre1.

RNA splicing (Q, blue bar) and RIDD cleavage (Figure 4F; Q, orange bar). Furthermore, STF treatment inhibited *XBP1* splicing (Figure 4F; Q + STF, blue bar), whereas cleavage of *BLOS1* RIDD RNA occurred normally even in the presence of STF (Figure 4F; Q + STF, orange bar), recapitulating our in vitro results (Figures 4B and 4D).

Thus, we tested the functional consequence of *XBP1* mRNA splicing inhibition, but leaving RIDD intact by examining the extent of cell death. Upon treatment of hyIRE1 cells with Q and STF, numbers of cells stained with Crystal violet were reduced (Figure 4G), and PARP cleavage was elevated (Figure 4H) when compared with those treated with Q alone, revealing that RIDD activation without *XBP1* splicing induces more predominant cell death. Similarly, we also tested the effect of STF on Q-activated mammalian cells carrying the endogenous WT IRE1 (Figures S4F–S4K), as we found that Q was able to activate hIre1for both *XBP1* RNA and *BLOS1* RNA cleavage in vitro (Figure S4E). Preferential inhibition of *XBP1* splicing but not RIDD brought by Q and STF resulted in more diminish numbers of crystal violet stained cells and increased PARP cleavage, in comparison to both *XBP1* splicing and RIDD activation in Q-treated cells (Figures S4I and S4J). Finally, experiments with *ire1* knockout MEFs conferred that the increase in apoptotic events observed in WT MEFs was an IRE1-dependent event (Figures S4K–S4M). Altogether, these findings, consistent with previous studies (Han et al., 2009; Upton et al., 2012), indicate that activation of RIDD without *XBP1* RNA promotes cell death.

DISCUSSION

Our data suggest that activated IRE1 RNase has different mechanisms for cleaving *XBP1*/*HAC1* RNA or RIDD substrates. Specifically, a catalytically active IRE1 unit engaged in *HAC1* or *XBP1* mRNA splicing is generated within the IRE1 oligomer, while IRE1 engaged in RIDD resides within an IRE1 monomer/dimer. An active catalytic core for *XBP1*/*HAC1* mRNA cleavage is unlikely to consist of all subunits within the IRE1 oligomer, but rather, oligomerization will lead to formation of the catalytically active pocket by establishing a specific orientation of catalytic residues. The structural conformation of the RNA binding and/or RNase catalytic residues within the catalytic core unit must differ such that *HAC1 or XBP1* RNA cannot compete the cleavage reaction of RIDD substrates and vice versa under single turnover conditions (Figures 1C–1G). Consistent with this idea, the Hill coefficient for IRE1 engaged in *HAC1* or *XBP1* RNA cleavage showed cooperativity among IRE1 subunits, while IRE1 engaged in RIDD cleavage displayed no significant cooperativity and may not form higher order structures as it does not require the $IF2^c$ (R1087) interface (Figures 3D–3F). It is possible, however, that IRE1 engaged in RIDD could also exist within an oligomer without any cooperative impact from other IRE1 subunits in the complex.

Structural and biochemical studies have revealed that the H1061 residue of yeast IRE1 plays a critical role in catalysis of *HAC1* cleavage (Korennykh et al., 2011). Similarly, we found that H1061 was also important for RIDD substrate cleavage (Figures 3B and S3G). Previous studies have also demonstrated that R1039 residue is involved in binding to *HAC1* RNA (Korennykh et al., 2011). Mutation of R1039 to Alanine did not affect ability of yIre1 to cleave RIDD substrate, while it decreased that of *HAC1* RNA (Figure S4C). Curiously, comparisons of Ire1 structure bound to Q highlight a difference in the spatial orientation of R1039 residue (Figure 4C). The ability of an IRE1 RNase inhibitor STF-083010 (STF) to inhibit *HAC1* RNA cleavage occurred regardless of the side-chain orientation of R1039, while the cleavage of *BLOS1* RNA by Q-induced yIre1, but not by ADP-induced yIre1, was no longer inhibited by STF-083010 (Figures 4B and 4D). Together with the noncompetitive inhibition between RIDD and *HAC1* substrates under steady-state competition experiments, these results point that binding sites for *XBP1*/*HAC1* RNA and RIDD substrate may differ, while both reactions share a catalytic site, including H1061 residue. Future work will require understanding of how RIDD substrates bind to IRE1 at the molecular level.

Notably, our model for IRE1 activation is different from what has previously been proposed (Han et al., 2009) where higher ordered structures were assigned to the RIDD active form of IRE1. Experiments reported by Han et al. (2009) utilized murine I642G IRE1, a homolog of L745G yeast IRE1, that binds to a modified nucleotide, 1NM-PP1. Upon expressing I642G IRE1 in INS-1 cells, the addition of 1NM-PP1 (without ER stress induction) activated *XBP1* mRNA splicing but not RIDD. In INS-1 cells expressing WT IRE1, instead of I642G IRE1, both *XBP1* mRNA splicing and RIDD occurred. Since I642G IRE1 does not autophosphorylate, it was concluded that I642G hIRE1 was unable to perform RIDD due to the lack of both phosphorylation and its accompanying oligomerization. However, we found that L745G yIre1 itself, a yeast homolog of I642G IRE1, was active for RIDD in vitro upon binding to 1NM-PP1 (Figure 2E), revealing that a lack of RIDD may not be an intrinsic property of L745G (or I642G) IRE1. Further studies have also reported that I642G IRE1 is active for RIDD upon addition of 1NM-PP1 (Upton et al., 2012) and with ER stress when introduced into $ire1^{-/-}$ cells (Hollien et al., 2009). These experiments suggest that, in addition to the occupancy of the kinase nucleotide-binding pocket, the ER stress-induced conformational change of the cytosolic portion of IRE1 containing both kinase and RNase domains holds a key to activation of I642G IRE1. The importance of the conformational change(s) through the ER luminal, transmembrane, and linker domains for activation of IRE1 RNase has previously been described (Credle et al., 2005; Korennykh et al., 2009; Volmer et al., 2013; Zhou et al., 2006). Such conformational changes may also trigger oligomerization and ultimately full activation of IRE1. In vitro, L745G yIre1 binding to 1NM-PP1 caused a mobility shift to heavier fractions on a density gradient sedimentation assay similar to ADP-bound WT yIre1 (Papa et al., 2003), revealing that L745G yIre1 is capable of forming a higher order structure similar to WT yIre1 without the ER luminal domain.

Additionally, in these previous experiments (Han et al., 2009), I642G IRE1 was introduced into INS-1 cells that express the endogenous WT IRE1. Here, we demonstrated that even a catalytically inactive H1061N yIre1 could reconstitute WT yIRE1 present below its active concentration. Importantly, we demonstrate that at higher molar ratios of WT to mutant IRE1,

HAC1 cleavage but not RIDD can be reconstituted (Figure 3B), suggesting that overexpressing mutant IRE1 may favor *XBP1* splicing over RIDD. Finally, our results revealed that the *HAC1* RNA cleavage activity of yIre1 is intrinsically more active than RIDD (Figures S1F and S2A), and thus, comparisons of activities between different forms of IRE1 should be performed carefully. Future work will require more understanding of I642G/L745G mutant IRE1.

This report shows that RIDD can occur in yeast, *S. cerevisiae*. We have previously reported that the only RNA cleaved by IRE1 in yeast is *HAC1* RNA (Niwa et al., 2005). However, the yeast recombinant IRE1 used in the previous study differed slightly from the one used in this study, where the linker domain was shortened in the yIre1 used for this study. We and others have noted that yIre1 with the full-length linker domain is less active for *HAC1* RNA cleavage (Korennykh et al., 2009). In addition, yIre1 with the full-length linker domain does not show significant RIDD cleavage activity. The molecular reasons for this observation are not clear, but it is in agreement with recent studies highlighting the importance of the linker region (Volmer et al., 2013).

Since IRE1 exhibits dual RNase activities, this calls into question the role of RIDD in vivo. Previously, contributions of RIDD versus *XBP1* mRNA splicing in vivo were assessed by comparing *ire1* knockout and *xbp1* knockout cells with a rationale that subtracting the *XBP1* contribution in *xbp1* knockout cells would allow assessment of RIDD functions (Hur et al., 2012). However, since both unspliced and spliced *XBP1* mRNA is not present in *xbp1* knockout cells, results from this approach also include contributions from an absent unspliced XBP1 protein and changes in transcription due to a lack of *XBP1*, not simply from RIDD activation alone. Furthermore, while no additional IRE1 splicing substrate mRNA beyond *XBP1* has been identified, splicing of such RNA would take place normally in *xbp1* knockout cells. Initially, activation of the IRE1 branch of the UPR was thought to be protective by virtue of *XBP1* splicing (Lin et al., 2007). However, our finding that RIDD promotes cell death highlights the importance of re-evaluating the functional significance of IRE1 activation. In *S. pombe*, where either *HAC1* or *XBP1* is absent, making RIDD the sole function for IRE1, a recent report revealed that IRE1 cleaves *KAR2/BiP*, a homolog of GRP78, within its 3′ UTR as a RIDD substrate (Kimmig et al., 2012), resulting in increased translation, rather than degradation. In addition, the kinetics or intensity of RIDD versus *XBP1/HAC1* splicing may differ depending on the cell or tissue type and the nature of the ER stress and ultimately may change the overall outcomes. Thus, careful evaluation of both the mechanistic and functional consequences between RIDD activation versus *XBP1/HAC1* splicing will provide a greater understanding of how ER stress affects cell physiology and also provide rationales for development of drugs and more effective treatment strategies for ER stress-related diseases.

EXPERIMENTAL PROCEDURES

In vitro transcription of IRE1 substrates, protein purification, and in vitro nuclease assay; determination of Hill coefficient; and determination of XBP1 splicing and RIDD in vivo are described in the Supplemental Experimental Procedures.

Competition Assays and Michaelis-Menten Kinetics

For single-turnover conditions, reactions were set up by incubating 3 μM of yIre1 (Figures 1E and 1F) or 15 μM yIre1 (Figure 1G) with buffer followed by addition of unlabeled (cold) RNA at the indicated concentrations. To this reaction mixture, 0.5 nM (Figures 1E and 1F) or 0.25 nM (Figure 1G) of radiolabeled RNA substrate were added and incubated at 30°C for 5 min. Reactions were then started upon addition of 2 mM ADP and stopped at the indicated times, as described in in vitro nuclease assay (Supplemental Experimental Procedures). For steady-state competition, reactions were performed similarly, except that 0.1 μM yIre1 was used and the concentration of radiolabeled RNA substrate was varied from 0.05–1.50 nM, as indicated and competed with 1.5 μM cold RNA. Samples were analyzed on a 6% urea gel, and molar values for uncleaved and cleaved products were calculated as described above. Velocity (nM/s) was calculated with the slope of the linear regression line of the graph plotting cleaved substrate (nM) over time (s). To generate the Lineweaver-Burk plots, the reciprocal of substrate concentration was plotted against the reciprocal of the velocity. Linear regression trend lines were then generated and graphed in Figures 2A and 2B.

trans-Complementation Assay

For transcomplementation assays, in vitro nuclease reactions were set up with nuclease reaction buffer, 2mM ADP, and 0.083 μM of WT yIre1. At this concentration of WT yIre1, efficient cleavage of either *HAC1* or RIDD RNA did not take place (Figure 3B, lanes 1 and 7). H1061N yIre1 was added to the reaction at molar ratios of 1:1, 1:2, 1:4, 1:6, or 1:12 ([WT]:[H1061N]). Reactions were started upon addition of 0.5 nM radiolabeled substrate and proceeded for 10 min at 30°C.

SUPPLEMENTAL INFORMATION

Supplemental Information includes Supplemental Experimental Procedures and four figures and can be found with this article online at http://dx.doi.org/10.1016/j.celrep.2014.09.016.

ACKNOWLEDGMENTS

We are grateful to Drs. Douglass Forbes, Peter E. Geiduschek, and Andrew Shiau for many discussions throughout the course of this study and Drs. Forbes and Geiduschek for comments on the manuscript. This work was supported by NIH RO1GM087415 and the ACS 118765-RSG-10-027-01-CSM to M.N., PO1 CA-67166 to A.K., and NIH T32, UCSD/LIAI allergy postdoctoral training grant for A.T.

Received: March 25, 2014
Revised: August 4, 2014
Accepted: September 8, 2014
Published: October 30, 2014

REFERENCES

Ali, M.M., Bagratuni, T., Davenport, E.L., Nowak, P.R., Silva-Santisteban, M.C., Hardcastle, A., McAndrews, C., Rowlands, M.G., Morgan, G.J., Aherne, W., et al. (2011). Structure of the Ire1 autophosphorylation complex and implications for the unfolded protein response. EMBO J. *30*, 894–905.

Aragón, T., van Anken, E., Pincus, D., Serafimova, I.M., Korennykh, A.V., Rubio, C.A., and Walter, P. (2009). Messenger RNA targeting to endoplasmic reticulum stress signalling sites. Nature *457*, 736–740.

Calfon, M., Zeng, H., Urano, F., Till, J.H., Hubbard, S.R., Harding, H.P., Clark, S.G., and Ron, D. (2002). IRE1 couples endoplasmic reticulum load to secretory capacity by processing the XBP-1 mRNA. Nature *415*, 92–96.

Chawla, A., Chakrabarti, S., Ghosh, G., and Niwa, M. (2011). Attenuation of yeast UPR is essential for survival and is mediated by IRE1 kinase. J. Cell Biol. *193*, 41–50.

Credle, J.J., Finer-Moore, J.S., Papa, F.R., Stroud, R.M., and Walter, P. (2005). On the mechanism of sensing unfolded protein in the endoplasmic reticulum. Proc. Natl. Acad. Sci. USA *102*, 18773–18784.

Gasch, A.P., Spellman, P.T., Kao, C.M., Carmel-Harel, O., Eisen, M.B., Storz, G., Botstein, D., and Brown, P.O. (2000). Genomic expression programs in the response of yeast cells to environmental changes. Mol. Biol. Cell *11*, 4241–4257.

Gonzalez, T.N., Sidrauski, C., Dörfler, S., and Walter, P. (1999). Mechanism of non-spliceosomal mRNA splicing in the unfolded protein response pathway. EMBO J. *18*, 3119–3132.

Han, D., Lerner, A.G., Vande Walle, L., Upton, J.P., Xu, W., Hagen, A., Backes, B.J., Oakes, S.A., and Papa, F.R. (2009). IRE1alpha kinase activation modes control alternate endoribonuclease outputs to determine divergent cell fates. Cell *138*, 562–575.

Hollien, J., and Weissman, J.S. (2006). Decay of endoplasmic reticulum-localized mRNAs during the unfolded protein response. Science *313*, 104–107.

Hollien, J., Lin, J.H., Li, H., Stevens, N., Walter, P., and Weissman, J.S. (2009). Regulated Ire1-dependent decay of messenger RNAs in mammalian cells. J. Cell Biol. *186*, 323–331.

Hur, K.Y., So, J.S., Ruda, V., Frank-Kamenetsky, M., Fitzgerald, K., Koteliansky, V., Iwawaki, T., Glimcher, L.H., and Lee, A.H. (2012). IRE1α activation protects mice against acetaminophen-induced hepatotoxicity. J. Exp. Med. *209*, 307–318.

Ishiwata-Kimata, Y., Promlek, T., Kohno, K., and Kimata, Y. (2013). BiP-bound and nonclustered mode of Ire1 evokes a weak but sustained unfolded protein response. Genes to cells: devoted to molecular & cellular mechanisms *18*, 288–301.

Kawahara, T., Yanagi, H., Yura, T., and Mori, K. (1997). Endoplasmic reticulum stress-induced mRNA splicing permits synthesis of transcription factor Hac1p/Ern4p that activates the unfolded protein response. Mol. Biol. Cell *8*, 1845–1862.

Kimmig, P., Diaz, M., Zheng, J., Williams, C.C., Lang, A., Aragón, T., Li, H., and Walter, P. (2012). The unfolded protein response in fission yeast modulates stability of select mRNAs to maintain protein homeostasis. eLife *1*, e00048.

Korennykh, A.V., Egea, P.F., Korostelev, A.A., Finer-Moore, J., Zhang, C., Shokat, K.M., Stroud, R.M., and Walter, P. (2009). The unfolded protein response signals through high-order assembly of Ire1. Nature *457*, 687–693.

Korennykh, A.V., Korostelev, A.A., Egea, P.F., Finer-Moore, J., Stroud, R.M., Zhang, C., Shokat, K.M., and Walter, P. (2011). Structural and functional basis for RNA cleavage by Ire1. BMC Biol. *9*, 47.

Lee, K.P., Dey, M., Neculai, D., Cao, C., Dever, T.E., and Sicheri, F. (2008). Structure of the dual enzyme Ire1 reveals the basis for catalysis and regulation in nonconventional RNA splicing. Cell *132*, 89–100.

Li, H., Korennykh, A.V., Behrman, S.L., and Walter, P. (2010). Mammalian endoplasmic reticulum stress sensor IRE1 signals by dynamic clustering. Proc. Natl. Acad. Sci. USA *107*, 16113–16118.

Lin, J.H., Li, H., Yasumura, D., Cohen, H.R., Zhang, C., Panning, B., Shokat, K.M., Lavail, M.M., and Walter, P. (2007). IRE1 signaling affects cell fate during the unfolded protein response. Science *318*, 944–949.

Lu, Y., Liang, F.X., and Wang, X. (2014). A synthetic biology approach identifies the mammalian UPR RNA ligase RtcB. Mol. Cell *55*, 758–770.

Mishiba, K., Nagashima, Y., Suzuki, E., Hayashi, N., Ogata, Y., Shimada, Y., and Koizumi, N. (2013). Defects in IRE1 enhance cell death and fail to degrade mRNAs encoding secretory pathway proteins in the Arabidopsis unfolded protein response. Proc. Natl. Acad. Sci. USA *110*, 5713–5718.

Niwa, M., Patil, C.K., DeRisi, J., and Walter, P. (2005). Genome-scale approaches for discovering novel nonconventional splicing substrates of the Ire1 nuclease. Genome Biol. *6*, R3.

Papa, F.R., Zhang, C., Shokat, K., and Walter, P. (2003). Bypassing a kinase activity with an ATP-competitive drug. Science *302*, 1533–1537.

Papandreou, I., Denko, N.C., Olson, M., Van Melckebeke, H., Lust, S., Tam, A., Solow-Cordero, D.E., Bouley, D.M., Offner, F., Niwa, M., and Koong, A.C. (2011). Identification of an Ire1alpha endonuclease specific inhibitor with cytotoxic activity against human multiple myeloma. Blood *117*, 1311–1314.

Sidrauski, C., Cox, J.S., and Walter, P. (1996). tRNA ligase is required for regulated mRNA splicing in the unfolded protein response. Cell *87*, 405–413.

Sidrauski, C., and Walter, P. (1997). The transmembrane kinase Ire1p is a site-specific endonuclease that initiates mRNA splicing in the unfolded protein response. Cell *90*, 1031–1039.

Travers, K.J., Patil, C.K., Wodicka, L., Lockhart, D.J., Weissman, J.S., and Walter, P. (2000). Functional and genomic analyses reveal an essential coordination between the unfolded protein response and ER-associated degradation. Cell *101*, 249–258.

Upton, J.P., Wang, L., Han, D., Wang, E.S., Huskey, N.E., Lim, L., Truitt, M., McManus, M.T., Ruggero, D., Goga, A., et al. (2012). IRE1α cleaves select microRNAs during ER stress to derepress translation of proapoptotic Caspase-2. Science *338*, 818–822.

Volmer, R., van der Ploeg, K., and Ron, D. (2013). Membrane lipid saturation activates endoplasmic reticulum unfolded protein response transducers through their transmembrane domains. Proc. Natl. Acad. Sci. USA *110*, 4628–4633.

Wiseman, R.L., Zhang, Y., Lee, K.P., Harding, H.P., Haynes, C.M., Price, J., Sicheri, F., and Ron, D. (2010). Flavonol activation defines an unanticipated ligand-binding site in the kinase-RNase domain of IRE1. Mol. Cell *38*, 291–304.

Yang, W. (2011). Nucleases: diversity of structure, function and mechanism. Q. Rev. Biophys. *44*, 1–93.

Zhou, J., Liu, C.Y., Back, S.H., Clark, R.L., Peisach, D., Xu, Z., and Kaufman, R.J. (2006). The crystal structure of human IRE1 luminal domain reveals a conserved dimerization interface required for activation of the unfolded protein response. Proc. Natl. Acad. Sci. USA *103*, 14343–14348.

Cell Reports, Volume *9*

Supplemental Information

Ire1 Has Distinct Catalytic Mechanisms for *HAC1* Splicing and RIDD

Arvin B. Tam, Albert C. Koong, and Maho Niwa

Figure S1

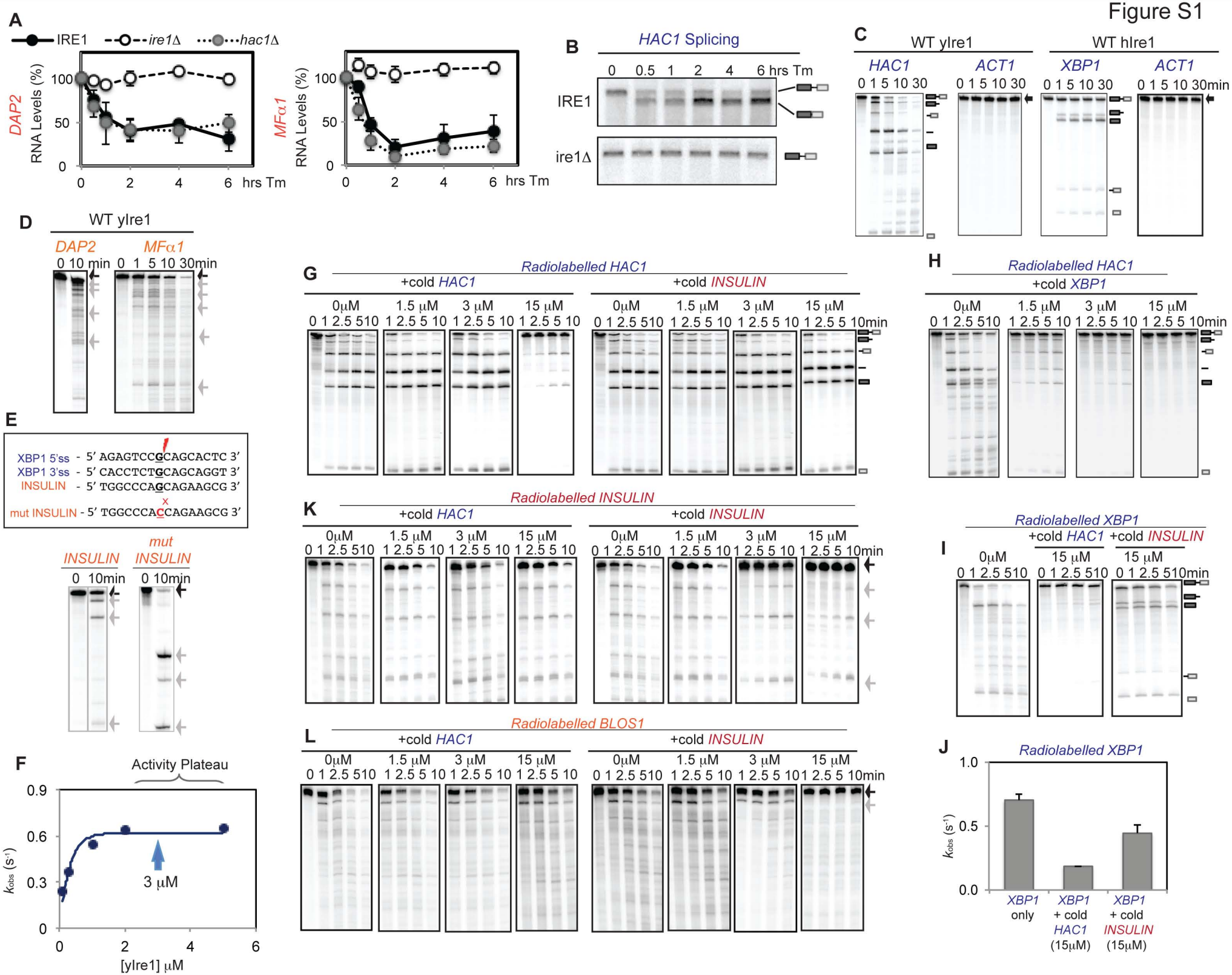
A
IRE1
ire1Δ
hac1Δ
DAP2
RNA Levels (%)
100
50
0
0 2 4 6 hrs Tm
MFα1
RNA Levels (%)
100
50
0
0 2 4 6 hrs Tm
B
HAC1 Splicing
0 0.5 1 2 4 6 hrs Tm
IRE1
ire1Δ
C
WT yIre1
HAC1
0 1 5 10 30
ACT1
0 1 5 10 30
WT hIre1
XBP1
0 1 5 10 30
ACT1
0 1 5 10 30min
D
WT yIre1
DAP2
0 10 min
MFα1
0 1 5 10 30min
E
XBP1 5'ss - 5' AGAGTCCGCAGCACTC 3'
XBP1 3'ss - 5' CACCTCTGCAGCAGGT 3'
INSULIN - 5' TGGCCCAGCAGAAGCG 3'
mut INSULIN - 5' TGGCCCACCAGAAGCG 3'
INSULIN
0 10min
mut INSULIN
0 10min
F
Activity Plateau
0.9
0.6
0.3
0
kobs (s-1)
3 μM
0 2 4 6
[yIre1] μM
G
Radiolabelled HAC1
+cold HAC1
+cold INSULIN
0μM 1.5 μM 3 μM 15 μM
0 1 2.5 5 10 1 2.5 5 10 1 2.5 5 10 1 2.5 5 10
0μM 1.5 μM 3 μM 15 μM
0 1 2.5 5 10 1 2.5 5 10 1 2.5 5 10 1 2.5 5 10min
H
Radiolabelled HAC1
+cold XBP1
0μM 1.5 μM 3 μM 15 μM
0 1 2.5 5 10 1 2.5 5 10 1 2.5 5 10 1 2.5 5 10min
K
Radiolabelled INSULIN
+cold HAC1
+cold INSULIN
0μM 1.5 μM 3 μM 15 μM
0 1 2.5 5 10 1 2.5 5 10 1 2.5 5 10 1 2.5 5 10
0μM 1.5 μM 3 μM 15 μM
0 1 2.5 5 10 1 2.5 5 10 1 2.5 5 10 1 2.5 5 10min
I
Radiolabelled XBP1
+cold HAC1
+cold INSULIN
0μM 15 μM 15 μM
0 1 2.5 5 10 0 1 2.5 5 10 0 1 2.5 5 10min
L
Radiolabelled BLOS1
+cold HAC1
+cold INSULIN
0μM 1.5 μM 3 μM 15 μM
0 1 2.5 5 10 1 2.5 5 10 1 2.5 5 10 1 2.5 5 10
0μM 1.5 μM 3 μM 15 μM
0 1 2.5 5 10 1 2.5 5 10 1 2.5 5 10 1 2.5 5 10min
J
Radiolabelled XBP1
1.0
0.5
0.0
kobs (s-1)
XBP1 only
XBP1 + cold HAC1 (15μM)
XBP1 + cold INSULIN (15μM)

Figure S2

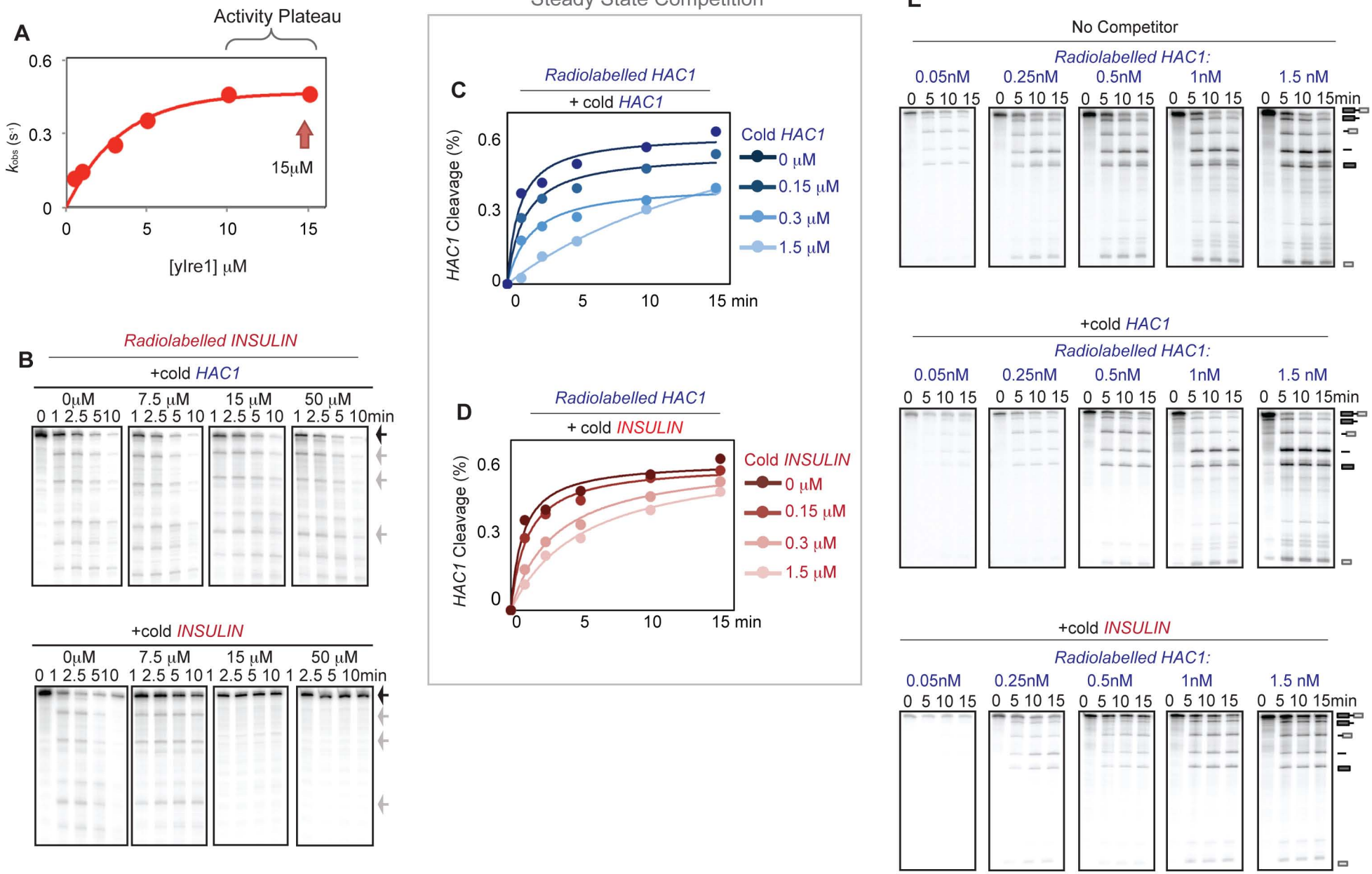
A
Activity Plateau
0.6
0.3
0
k_{obs} (s^{-1})
15μM
0
5
10
15
[ylre1] μM
B
Radiolabelled INSULIN
+cold HAC1
0μM
7.5 μM
15 μM
50 μM
0 1 2.5 5 10
1 2.5 5 10
1 2.5 5 10
1 2.5 5 10min
+cold INSULIN
0μM
7.5 μM
15 μM
50 μM
0 1 2.5 5 10
1 2.5 5 10
1 2.5 5 10
1 2.5 5 10min
Steady State Competition
C
Radiolabelled HAC1
+ cold HAC1
HAC1 Cleavage (%)
0.6
0.3
0
0
5
10
15 min
Cold HAC1
0 μM
0.15 μM
0.3 μM
1.5 μM
D
Radiolabelled HAC1
+ cold INSULIN
HAC1 Cleavage (%)
0.6
0.3
0
0
5
10
15 min
Cold INSULIN
0 μM
0.15 μM
0.3 μM
1.5 μM
E
No Competitor
Radiolabelled HAC1:
0.05nM
0.25nM
0.5nM
1nM
1.5 nM
0 5 10 15
0 5 10 15
0 5 10 15
0 5 10 15
0 5 10 15min
+cold HAC1
Radiolabelled HAC1:
0.05nM
0.25nM
0.5nM
1nM
1.5 nM
0 5 10 15
0 5 10 15
0 5 10 15
0 5 10 15
0 5 10 15min
+cold INSULIN
Radiolabelled HAC1:
0.05nM
0.25nM
0.5nM
1nM
1.5 nM
0 5 10 15
0 5 10 15
0 5 10 15
0 5 10 15
0 5 10 15min

Figure S3

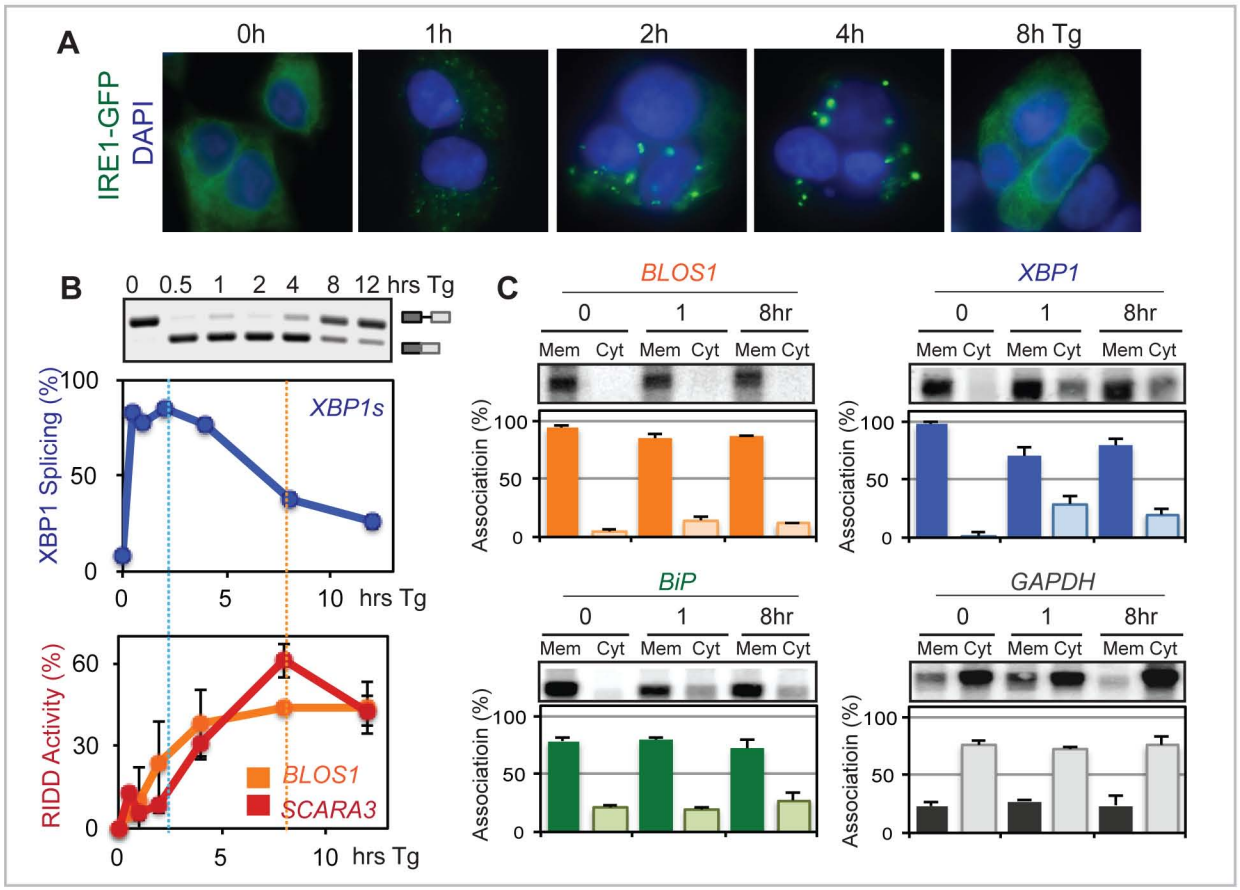
A
0h
1h
2h
4h
8h Tg
IRE1-GFP
DAPI
B
0 0.5 1 2 4 8 12 hrs Tg
XBP1 Splicing (%)
XBP1s
hrs Tg
RIDD Activity (%)
BLOS1
SCARA3
C
BLOS1
XBP1
BiP
GAPDH
0
1
8hr
Mem Cyt
Association (%)

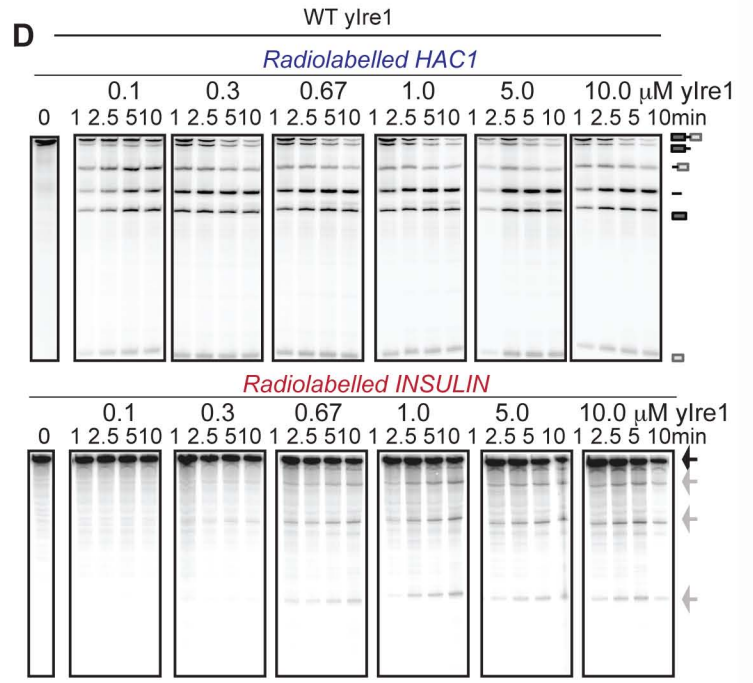
D
WT yIre1
Radiolabelled HAC1
0.1 0.3 0.67 1.0 5.0 10.0 μM yIre1
0 1 2.5 5 10 1 2.5 5 10 1 2.5 5 10 1 2.5 5 10 1 2.5 5 10 1 2.5 5 10min
Radiolabelled INSULIN

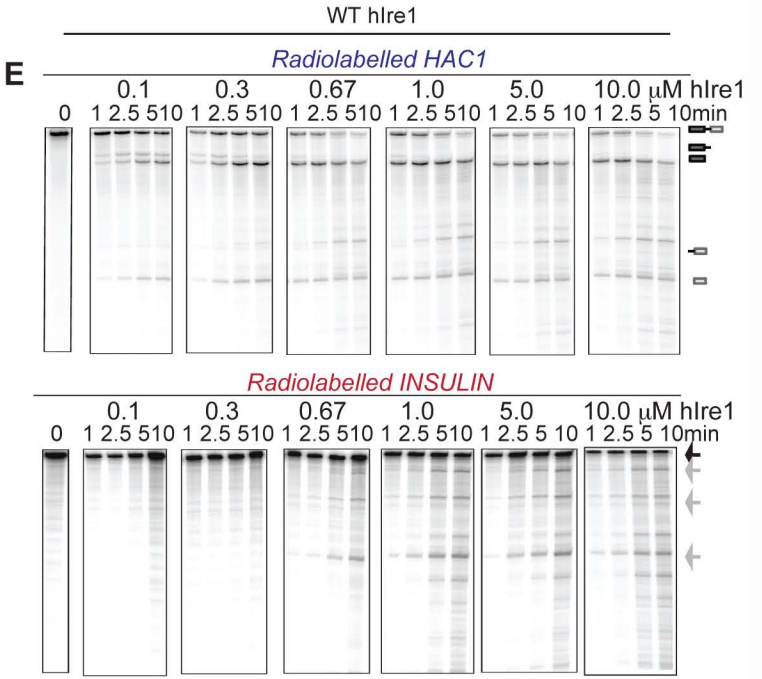
WT hIre1
E
Radiolabelled HAC1
0.1 0.3 0.67 1.0 5.0 10.0 μM hIre1
0 1 2.5 5 10 1 2.5 5 10 1 2.5 5 10 1 2.5 5 10 1 2.5 5 10 1 2.5 5 10min
Radiolabelled INSULIN

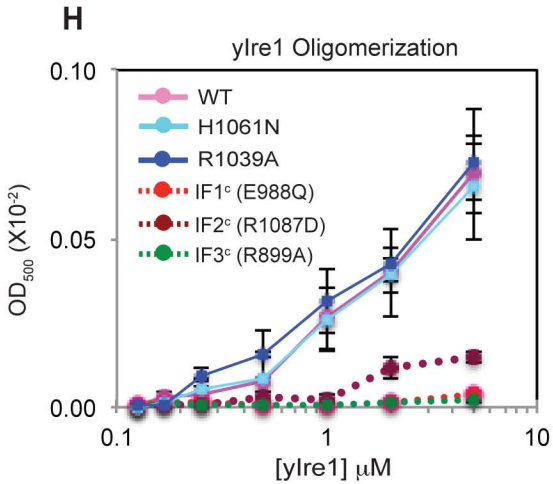
H
yIre1 Oligomerization
WT
H1061N
R1039A
IF1c (E988Q)
IF2c (R1087D)
IF3c (R899A)
OD500 (X10-2)
[yIre1] μM

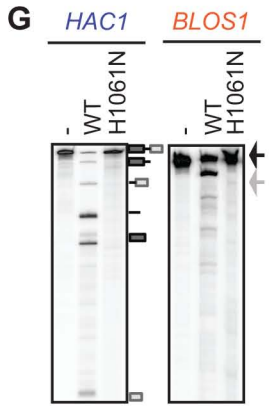
G
HAC1
BLOS1
-
WT
H1061N

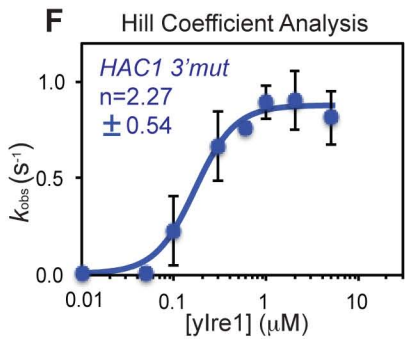
F
Hill Coefficient Analysis
HAC1 3'mut
n=2.27
±0.54
kobs (s-1)
[yIre1] (μM)

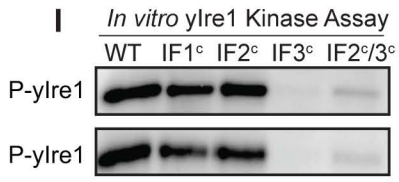
I
In vitro yIre1 Kinase Assay
WT IF1c IF2c IF3c IF2c/3c
P-yIre1
P-yIre1

Figure S4

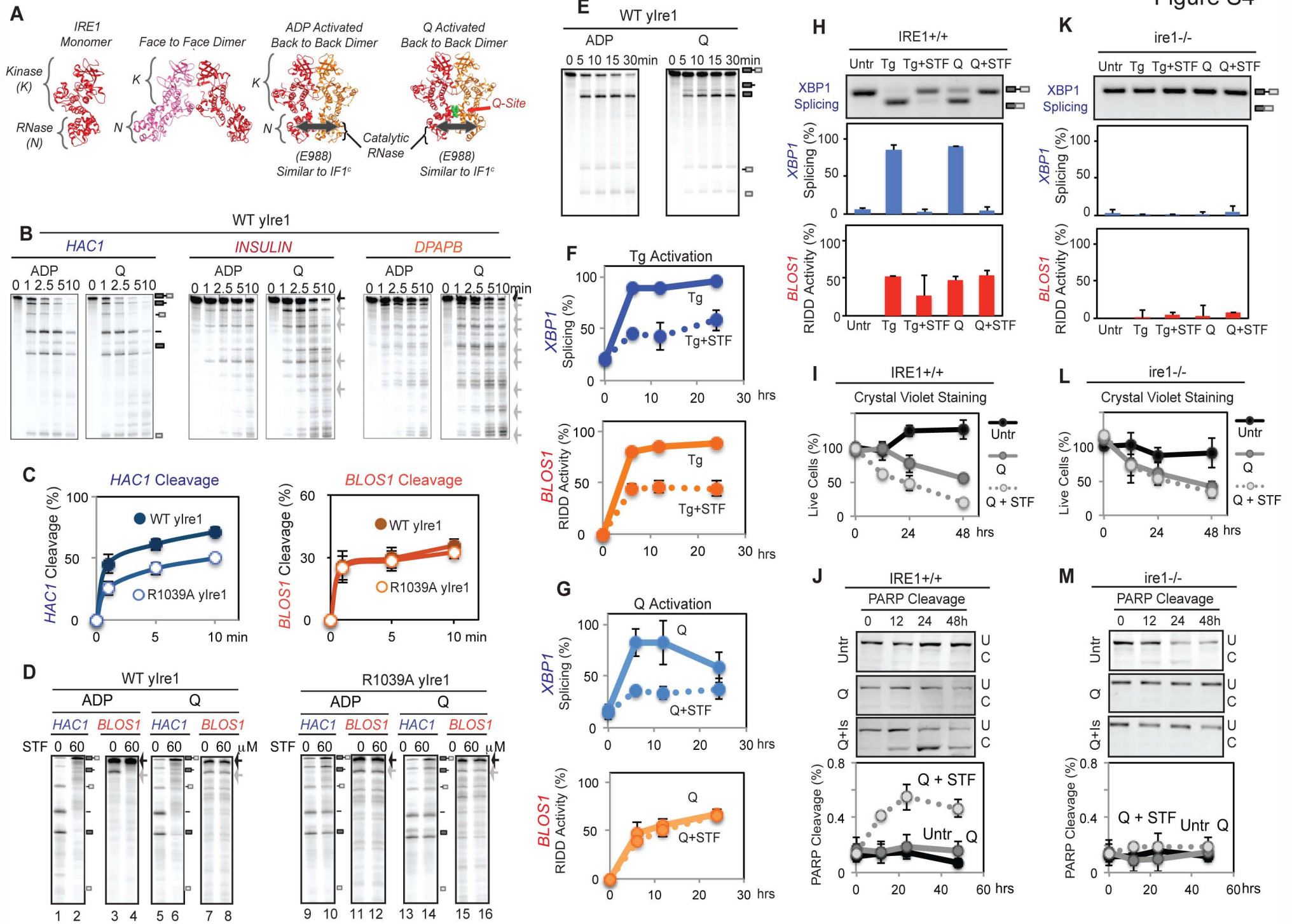
A
IRE1 Monomer
Face to Face Dimer
ADP Activated Back to Back Dimer
Q Activated Back to Back Dimer
Kinase (K)
RNase (N)
K
N
Catalytic RNase
Q-Site
(E988) Similar to IF1c
B
WT yIre1
HAC1
INSULIN
DPAPB
ADP
Q
0 1 2.5 5 10
min
C
HAC1 Cleavage
BLOS1 Cleavage
HAC1 Cleavage (%)
BLOS1 Cleavage (%)
WT yIre1
R1039A yIre1
min
D
WT yIre1
R1039A yIre1
ADP
Q
HAC1
BLOS1
STF 0 60
0 60 µM
1 2 3 4 5 6 7 8 9 10 11 12 13 14 15 16
E
WT yIre1
ADP
Q
0 5 10 15 30min
F
Tg Activation
XBP1 Splicing (%)
BLOS1 RIDD Activity (%)
Tg
Tg+STF
hrs
G
Q Activation
Q
Q+STF
H
IRE1+/+
Untr Tg Tg+STF Q Q+STF
XBP1 Splicing
XBP1 Splicing (%)
BLOS1 RIDD Activity (%)
I
IRE1+/+
Crystal Violet Staining
Live Cells (%)
Untr
Q
Q + STF
hrs
J
IRE1+/+
PARP Cleavage
0 12 24 48h
Untr
Q
Q+Is
U
C
PARP Cleavage (%)
Q + STF
Untr Q
60 hrs
K
ire1-/-
L
ire1-/-
M
ire1-/-

SUPPLEMENTAL FIGURE LEGENDS

Figure *S1*. Yeast Ire1 performs RIDD both *in vivo* and *in vitro*

(Related to Figure 1)

(A) RIDD in yeast (*S. cerevisiae*) during ER stress. WT (closed circle), *ire1Δ* (open circle), or *hac1Δ* (grey circle) cells were treated with tunicamycin (Tm) for up to 6 hrs and RNA was collected. RNA levels of *DAP2* and *MFα1* were determined by reverse transcription-followed by quantitative PCR (RT-qPCR). RNA decreased during ER stress only in WT and *hac1Δ* cells and not in *ire1Δ*, indicating RIDD where the decrease in RNA is IRE1 dependent, but HAC1 independent. Error bars shown in Figure *S1* all represent data from at least three independent repeats.

(B) *HAC1* Splicing in wild type IRE1 and *ire1Δ* strains during ER stress. The same RNA isolated from (A) was analyzed for *HAC1* splicing by Northern Blot. Un-spliced (top band) and spliced (bottom band) are indicated. *HAC1* splicing occurred only in WT cells and not in *ire1Δ* cells. *hac1Δ* cells did not show any *HAC1* signal by Northern Blot as anticipated (data not shown).

(C) *In vitro* cleavage of *HAC1/XBP1* by purified recombinant WT yeast IRE1 (yIre1) or human IRE1 (hIre1) as indicated. *In vitro* transcribed radiolabeled *HAC1*, *XBP1, or ACT1* RNA was incubated with 1μM WT yIre1 or WT hIre1 for up to 30 min upon addition of 2mM ADP. Cleavage fragments were analyzed by separation on a denaturing Urea 6% polyacrylamide gel. *HAC1* and *XBP1* RNA were cleaved by yIre1 and hIre1, respectively, whereas *ACTIN* RNA was cleaved by neither yIre1 nor hIre1.

(D) WT yIre1 cleaved *DAP2* or MFα1 RNA *in vitro*. Nuclease assays were performed using 1μM WT yIre1 and *in vitro* transcribed *DAP2* or MFα1 radiolabeled RNA. Cleavage fragments were analyzed upon incubation with ADP for indicated length of time. Uncut precursor is shown as black arrows and cleavage fragments are indicated with gray arrows.

(E) The invariant '**G**' residue critical for IRE1 cleavage present in *XBP1* mRNA 5' and 3' splice sites (5'SS and 3'SS) (Sidrauski and Walter, 1997) and in WT *INSULIN* RNA (Han et al., 2009) is mutated to "C" in mutant *INSULIN* RNA (mut *INSULIN*) (top panel). Incubation of mut *INSULIN* with WT yIre1 and 2mM ADP for 10 min diminished the cleavage at this site, but instead activated alternative cleavage sites.

(F) Activation Profile of yIre1 *in vitro*. To determine single turnover reaction conditions, *HAC1* RNA cleavage reactions were performed with the increasing concentrations of yIre1 ranging from 0.1-5 μM until there was no further increase in *HAC1* RNA cleavage activity. k_{obs} (s^{-1}) for *HAC1* RNA cleavage reaction at different concentration of yIre1 was calculated from profiles of % cleavage of *HAC1* RNA throughout time courses performed at different concentrations of yIre1. k_{obs} (s^{-1}) stayed at similar values when concentration of yIre1 became higher than 1μM and thus, we chose 3μM Ire1 for the subsequent competition experiments as a single turnover condition.

(G-H) Competition assays described in Figure 1C-1E. Reactions were performed with radiolabeled *HAC1* and 3μM yIre1 with increasing amounts of either cold (unlabeled) *HAC1* or cold *INSULIN* RNA (G) or cold *XBP1* RNA (H), as indicated.

(I-J) *XBP1* RNA cleavage by hIre1 was effectively competed by *HAC1* RNA but not *INSULIN* (RIDD) RNA. Competition assays were performed with radiolabeled *XBP1* RNA and 3μM yIre1 with 15 μM of either cold *HAC1* or cold *INSULIN* RNA. k_{obs} was calculated from reactions shown in I (J).

(K-L) Competition assays described in Figure 1F. Reactions were performed with radiolabeled *INSULIN* (K) or *BLOS1* (L) and 3μM yIre1 with increasing amounts of either cold *HAC1* or cold *INSULIN* RNA, as indicated.

Figure *S2*. Competition Assays of RIDD at Single Turnover and Steady State Conditions
(Related to Figures 1 and 2)

(A) Activity profile for RIDD. Similarly to Figure *S1F*, *INSULIN* RNA cleavage were performed with increasing concentration of yIre1 ranging from 0.1-15 μM using 0.25nM radiolabeled *INSULIN*. At 10μM of yIre1, there was no further increase in k_{obs} (s^{-1}) for *INSULIN* RNA cleavage activity. At 15μM of yIre1, competition experiments of radiolabeled *INSULIN* RNA were repeated with either cold *HAC1* or *INSULIN* RNA (Figure 1G).

(B) *INSULIN* RNA cleavage (RIDD substrate cleavage) by yIre1 was competed by cold *INSULIN* RNA but not by cold *HAC1* RNA using 15μM yIre1 cleaving 0.25nM radiolabeled *INSULIN* RNA. Competition experiments were performed with 0, 7.5, 15 or 50μM cold *HAC1* or *INSULIN* RNA. k_{obs} for these reactions are graphed in Figure 1G.

(C-D) Steady state competition experiments of radiolabeled *HAC1* RNA cleavage. To achieve steady state conditions, lower concentration of yIre1 (0.1 μM) was incubated with varying concentrations of either cold *HAC1* (C) or cold *INSULIN* (D) RNA competitors at 0, 0.15, 0.3, or 1.5μM and incubated with 2mM ADP for up to 15 min. % *HAC1* cleaved was calculated and graphed. Addition of 0.15, 0.3 or 1.5μM cold *HAC1* competitor resulted in a decrease in activity, while addition of 0.3 or 1.5μM cold *INSULIN* competitor also resulted in decreased activity.

(E) Non-competitive inhibition of *HAC1* RNA cleavage by RIDD RNA. Using steady state conditions described in (C) and (D), increasing concentrations of radiolabeled *HAC1* (ranging from 0.05-1.5nM) were incubated with 0.1μM yIre1 in the presence of no competitor, 1.5μM cold *HAC1* or cold *INSULIN* RNA. Results are shown as a Lineweaver-Burk plot and described in Figures 2A and 2B.

Figure *S3*. RIDD cleavage does not require IRE1 oligomerization
(Related to Figure 3)

(A) Formation of hIRE1 foci correlate with *XBP1* mRNA splicing but not with RIDD. HEK293 cells stably expressed hIRE1-GFP (Li et al., 2010) were treated with 200nM thapsigargin (Tg) for up to 8 hrs and visualized for IRE1 (green). Human IRE1 formed visible foci at 1, 2 and 4 hr time points, but dispersed by 8 hr. DAPI staining (blue) shows nucleus.

(B) Kinetics of *XBP1* mRNA splicing and RIDD activity in HEK293 cells when treated with Tg (200nM). Cells were collected at the indicated times and RNA was examined by reverse transcription (RT)-PCR to determine the percentage of spliced *XBP1* mRNA by gel-electrophoresis with un-spliced and spliced *XBP1* indicated (top panel). *XBP1* splicing was calculated by (spliced *XBP1*/(spliced + unspliced *XBP1* mRNA) X100%. The same cDNA was used to perform quantitative PCR (qPCR) using primers complimentary to *BLOS1* (orange) and *SCARA3* (dark red) mRNA, another RIDD target (Hollien et al., 2009). RIDD activity was calculated using [(*RIDD* mRNA in untreated cells - *RIDD* in treated cells) / *RIDD* in untreated cells] X100%. Blue line indicates high *XBP1* splicing activity at 2 hrs, while the orange & dark red lines indicate the peak of RIDD activity at 8 hrs. Error bars were generated from at least three independent experiments. It should be noted that *XBP1* mRNA splicing activity includes both IRE1 cleavage of the *XBP1* intron and the exon ligation steps, while RIDD activity includes degradation of IRE1 cleaved RNA fragments. Thus, the apparent kinetic relationships of *XBP1* mRNA splicing and RIDD may over-estimate kinetic differences of IRE1-dependent steps alone in HEK293 cells. This may also contribute differential kinetic relationships of *XBP1/HAC1* and RIDD substrate RNA cleavage observed

in vivo vs *in vitro* where both cleavage reactions occurred with similar kinetics (Figures 1A, S1C, S1D). Alternatively, an additional factor(s) may exist to modulate IRE1 cleavage of either *HAC/XBP1* or RIDD substrate RNA *in vivo*.

(C) Localization of IRE1 RNA substrates. Both *XBP1* and RIDD substrate RNA were associated with ER membrane prior to ER stress induction. HEK293 cells were treated with 200nM Tg for up to 8hrs, and cytosol (Cyt) and ER membrane (Mem) fractions were separated using serial detergent extractions as described in (Stephens et al., 2005). RNAs isolated from these fractions were analyzed by Northern blots probing *BLOS1*, *XBP1,* and *KAR2/BIP* mRNA. Most of both *XBP1* and *BLOS1* RNA were localized to the ER membrane even prior to UPR induction (compare RNA in the untreated (0) vs Tg treated cells for 1 or 8 hrs). As reported previously, splicing released *XBP1* mRNA into the soluble cytoplasmic fraction (Stephens et al., 2005). In contrast, the majority of *GAPDH* mRNA was localized to the cytosolic fraction. Consistent with previous reports, some GAPDH was found in the membrane fraction (Stephens et al., 2005). Standard deviations were calculated from at least three independent experiments.

(D-E) To determine Hill Coefficients, increasing amounts of either yIre1 (D) or hIre1 (E) were used to perform nuclease reactions (Korennykh et al., 2009). Un-cleaved and cleaved fragments of RNA were indicated. k_{obs} (s^{-1}) were graphed in Figures 3A.

(F) Hill coefficient analysis for *HAC1* with the 3' stem loop mutated (*HAC1 3'* mutant). The 3' stem loop mutation has been shown to block cleavage by IRE1 (Sidrauski and Walter, 1997). Nuclease reactions described in (D) were done using *HAC1* 3' mutant. Hill Coefficients for *HAC1* 3' mutant (2.27±0.54) is similar to unmodified WT *HAC1* (2.13±0.38), indicating that both are cooperative and that numbers of the cleavage sites do not affect the Hill Coefficients.

(G) H1061N yIre1 is nuclease dead for both *HAC1* RNA cleavage and RIDD. Either WT yIre1 or H1061N yIre1 was activated with 2mM ADP for 15 min allowing the cleavage of either *HAC1* or *BLOS1* RNA.

(H) Oligomerization assays as described in (Korennykh et al., 2009) was performed on either WT yIre1, H1061N or R1039A mutants, or interface mutants $IF1^c$, $IF2^c$, and $IF3^c$. At increasing concentrations, WT yIre1, H1061N yIre1 and R1039A yIre1 showed significant increases in OD_{500}, while OD_{500} for $IF1^c$, $IF2^c$ and $IF3^c$ yIre1 mutants did not show such increase. WT yIre1 (solid pink), H1061N yIre1 (solid light blue), R1039A yIre1 (solid dark blue), $IF1^c$ mutant E988Q yIre1 (dotted red), $IF2^c$ mutant R1087D yIre1 (dotted maroon), $IF3^c$ mutant R899A yIre1 (dotted green) are shown.

(I) *In vitro* kinase assay for Ire1 oligomerization mutants. WT and interface mutants $IF1^c$ (E988Q), $IF2^c$(R1087D), $IF3^c$ (R899A), or a $IF2^c/IF3^c$ double interface mutant were tested for their abilities to undergo autophosphorylation in *in vitro. In vitro* kinase reactions were performed upon incubation with γ^{32}P-ATP, and analyzed by SDD-PAGE, followed by autoradiography.

Figure S4. RIDD activation leads to apoptosis

(Related to Figure 4)

(A) Back to back dimer of IRE1 forms a catalytically active RNase site (Ali et al., 2011; Lee et al., 2008; Wiseman et al., 2010). An IRE1 monomer (red) containing the kinase and RNase domains is shown (Left). To initiate trans-autophosphorylation, two IRE1 monomers adopt a face to face conformation where the nucleotide binding pockets of each monomer can access the activation loop of the other (Ali et al., 2011). In the face-to-face dimer, the catalytic RNase sites are inactive and pointing away from each other, and face to face interactions were not present in the crystalized oligomer (Figure 3C). Formation of a back to back dimer where the nucleotide binding pockets are facing away from each other juxtaposes the RNase domains and forms an active nuclease site. Formation of the back-to-back dimer can be formed with ADP binding to the nucleotide pocket and with quercetin in the Q-site. The back-to-back dimer forms the building block of the IRE1 oligomer (Figure 3C) and the interface $IF1^c$ is indicated.

(B) Quercetin (Q) activation of RIDD. Incubation of yIre1 with Q (100μM) induced cleavage of *HAC1* RNA at kinetics and the extent similar to that by ADP. Q also induced Ire1 to cleave *INSULIN* or *DAP2* RIDD substrates efficiently *in vitro*. Precursor mRNA and cleavage products were indicated as previous figures. IRE1 dependent cleavage reactions of both *HAC1* and RIDD substrate RNA are faster with Q than ADP. This may be due to the ability of Q to form the back-to-back IRE1 dimer dimers (Figure S4A) (Wiseman et al., 2010), which would be a building unit for the fully active oligomerized IRE1. Though no cooporativity between IRE1 is involved (Figure 3A), the back-to-back dimer formation may help to stabilize a specific conformation of IRE1 needed for RIDD substrate cleavage.

(C) R1039A yIre1 was reduced for *HAC1* cleavage, but retained RIDD cleavage. 1μM of either WT yIre1 (closed circle) or R1039A yIre1 (open circle) was incubated with 2mM ADP for up to 10 min. An amino acid change at R1039 to Alanine decreased the ability of yIre1 to cleave *HAC1* RNA (left panel). On the other hand, it did not

show the significant change in *BLOS1* RNA (right panel) where both WT and R1039A yIre1 showed the same *BLOS1* RNA cleavage activity. Error bars represent data from at least three independent experiments.

(D) Representative RNase reactions for Figures 4D and 4E. WT yIre1 (1μM) was incubated with either ADP or Q for 30 min to cleave *HAC1* or *BLOS1* RNA, in the presence or absence of STF-083010 (Papandreou et al., 2011). *HAC1* RNA cleavage was effectively inhibited when 60μM STF-083010 (STF) was added (lanes 1&5 (no inhibition) vs 2&6 (with STF)). In contrast, *BLOS1* RNA cleavage was inhibited by STF when ADP was used as a cofactor (lane 4), but not inhibited when Q was added as a co-factor (lane 8). Additionally, similar experiments were performed with R1039A yIre1 (lanes 9-16). STF did not inhibit either *HAC1* or *BLOS1* RNA cleavage reactions.

(E) Quercetin (Q) activates hIre1 in *in vitro*. hIre1 was activated with either 2mM ADP or 100μM Q and incubated with radiolabeled *XBP1* in an *in vitro* nuclease reaction for the indicated length of time. Addition of Q alone activated hIre1 cleavage of *XBP1* RNA to a similar extent as ADP.

(F-G) Q activated RIDD is not inhibited by STF in wild type MEFs. Wild type MEFs were treated with 200nM thapsigargin (Tg) or Tg + 60μM STF (F), for up to 24 hrs. mRNA was isolated and levels of the spliced *XBP1* mRNA or *BLOS1* mRNA were determined by performing RT-PCR or RT-qPCR, respectively. STF inhibited *XBP1* mRNA splicing and cleavage of *BLOS1* RNA induced upon Tg treatment of cells. Similarly, wild type MEFs incubated with Q (450μM) (G) were also activated for *XBP1* splicing and RIDD. In this case, however, STF was unable to inhibit *BLOS1* RNA cleavage while *XBP1* splicing was effectively inhibited. Error bars represent at least three independent experiments. RIDD activity (%) was calculated as described before (Figure S3B).

(H)(K) STF inhibits *XBP1* mRNA splicing, but does not impact RIDD for Q-activated IRE1 *in vivo*. Mouse embryonic fibroblasts (MEFs) carrying WT mouse IRE1 (H) or *ire1* knockout (K) were incubated with Tg, Tg+STF , Q (450μM), and Q+STF or untreated for 2 hrs. RNA isolated from each reaction were analyzed by RT-qPCR for both *XBP1* splicing (H or K, top panel) and RIDD activity. Positions of spliced and un-spliced *XBP1* RNA were indicated. Quantitation of spliced *XBP1* RNA and *BLOS1* mRNA cleavage was shown.

(I)(L) WT IRE1 (I) or *ire1* knockout (L) MEFs were incubated with Q, Q+STF, or untreated for up to 48 hrs and stained with crystal violet. Numbers of cells stained with % of crystal violet (live cells) were calculated.

(J)(M) Upon treatment with Q, or Q+STF, or untreated WT-IRE1 cells (J) or *ire1* knockout MEFs (M) for indicated length of time, total cell extracts were prepared and examined for apoptosis by examining PARP cleavage upon performing western blots using anti-PARP antibody. Positions of uncleaved (U) and cleaved (C) PARP are indicated and quantitated to calculate % cleavage of PARP at each time point (bottom panel). Error bars represent at least three independent experiments.

SUPPLEMENTAL EXPERIMENTAL PROCEDURES

In Vitro IRE1 Substrates: HAC1, XBP1, and RIDD

HAC1 substrate (508 nt) used in all the *in vitro* RNase reactions was *in vitro* transcribed from a plasmid described previously (pCF187) (Sidrauski and Walter, 1997). Human *XBP1* substrate (444 nt) (Lee et al., 2002) was made by PCR amplifying human cDNA with primers containing a T7 site (F)-TAATACGACTCACTATAGGGAGAAGAACCAGGAGTTAAGAC; (R)-TAAGACTAGGGGCTTGGTATATATGTG. RIDD substrates were also prepared by PCR amplifying cDNA from the appropriate organism with primers containing a T7 site. *INSULIN* (mouse INSULIN-2) RNA (503 nt) was prepared as described (Han et al., 2009). *BLOS1* (mouse *BLOS1*) (379 nt) and yeast *DPAPB* (DAP2) (538 nt) substrate RNA was prepared from a DNA fragment prepared by PCR amplification using mouse or yeast cDNA, respectively, using the following primers: *BLOS1*: (F) ATGGTACCTAATACGACTCACTATAGGATGCTGTCCCGCCTGC, (R) ATGAGCTCCTAGGATGGTGCAGACTGCAG; *DAP2*: (F) ATGGTACCTAATACGACTCACTATAGGGCAGAAAAATGCGACAAAGG; (R) ATGAGCTCTTGAAATGTCTTCCGCCATC. PCR products were then phenol/chloroform extracted and ethanol precipitated and used as templates for *in vitro* transcription

In Vitro Transcription of RNA Substrates

In vitro transcription of radiolabeled RNA substrates has been described previously (Chawla et al., 2011; Sidrauski and Walter, 1997). Briefly, *in vitro* transcription was performed using T7 RNA polymerase (Promega) at 37 °C, 1mM each of ATP, CTP, GTP, 100μM of UTP, and 50 μCi of α^{32}P-UTP (3000Ci/mmol), and 1 μg of template DNA. Transcripts were separated on a 6% UREA-PAGE gel and radiolabeled RNA products were gel extracted by phenol/chloroform followed by ethanol precipitation. Activity of probes was measured by scintillation counter, and diluted to an activity of 20,000 cpm/μl, and based on the efficiency of the scintillation counter, this was equivalent to 10 fmol/μl of radiolabeled RNA.

Unlabeled (cold) RNA was transcribed using MEGAscript T7 Kit (Life Technologies) according to manufacturer's instructions, using 1μg of template DNA. To ensure that the cold RNA was equivalent to the radiolabeled RNA, cold RNA was gel purified side by side with its radiolabeled counterpart. Concentration was then determined upon quantitation by NanoDrop (Thermo).

Protein Purification and Site Directed Mutagenesis

For this study, we used a 6XHis-tagged WT yIre1 containing the entire cytosolic domain (642aa-1115aa) integrated into an expression vector (pET15b). Proteins were expressed in *E. coli* and purified using a Ni-NTA

column (Invitrogen) as described (Sidrauski and Walter, 1997). Recombinant human IRE1α (hIre1) was expressed and purified using a Baculovirus SF-9 expression system and purified using a Ni-NTA column, as previously described (Niwa et al., 1999). Point mutations in yIre1 were generated using QuickChange Site Directed Mutagenesis (Stratagene/Agilent) according to manufacturer's instructions using the plasmid containing WT yIre1 (642-1115), and point mutations were confirmed by sequencing.

In vitro Nuclease Assay and Kinetic Analysis

In vitro nuclease assays were performed as described in (Sidrauski and Walter, 1997). Reactions were performed in a 20 µl volume in nuclease reaction buffer (40mM Hepes, 7.0, 10mM $Mg(OAc)_2$, 50mM KOAc, 5mM DTT) at 30°C for the indicated amount of time, unless otherwise indicated. Standard nuclease reactions contained 2mM ADP, 100µM quercetin (Sigma) or 60µM STF-083010 (Papandreou et al., 2011) when indicated, 1µM either yIre1 or hIre1, and 0.5nM radiolabeled RNA. For reactions with L745G yIre1, 20µM 1NM-PP1 (Calbiochem) was used. Reactions were started when radiolabeled substrate was added, and reactions were stopped by addition of stop buffer (7M Urea, 350mM NaCl, 10mM Tris pH 7.6, 10mM EDTA, 1% SDS) and RNA was extracted using phenol/chloroform, ethanol precipitated, and analyzed on a denaturing 6% Urea acrylamide gel. To determine reaction rates, signal from each lane was quantified using Typhoon 9400 (GE Healthcare) and analyzed using ImageQuant (GE Healthcare). Based on the numbers of the U residues in individual cleaved fragments, we calculated the molar concentration of each cleavage products. % cleavage for *HAC1, XBP1* or RIDD RNA was calculated as [(sum of cleaved RNA fragments) / (uncleaved RNA + sum of cleaved RNA fragments)] X100%. For each time course, an activation curve was generated by plotting time (x) vs. cleaved substrate (y). Using this data, non-linear regression analysis was performed in SigmaPlot (Systat Software, Inc) to generate a curve using the exponential curves function. k_{obs} was generated using the initial slope of the generated curve obtained in SigmaPlot.

Determination of Hill Coefficients

Hill Coefficients were determined as previously described in (Korennykh et al., 2009). Briefly, standard nuclease assays were set up with nuclease buffer, 2mM ADP, and varying concentrations of either yIre1 or hIre1, as described. Reactions were performed in 20µl, and started when 0.5nM radiolabeled RNA (either *HAC1, INSULIN, HAC1 3' mut* for yIre1 or *XBP1, INSULIN* for hIre1) was added. Reactions were stopped with stop buffer and analyzed on 6% UREA gel, and molar values for uncleaved and cleaved products were calculated. For each concentration of Ire1, k_{obs} was calculated as described above and values were plotted ([Ire1] vs k_{obs}) and fitted using GraphPad Prism 5 (La Jolla, CA). The Hill coefficient was calculated by Prism using a four parameter logistic equation under the sigmoidal dose response curve with variable slope function. We interpret a

non-cooperative Hill coefficient of 1 as IRE1 acting within a dimer since monomeric IRE1 is inactive (Lee et al., 2008). Experiments were done at least three times with standard deviations shown.

Structural Analysis of IRE1

Structural analysis was done using Chimera (http://www.cgl.ucsf.edu/chimera) (Pettersen et al., 2004) and structure prediction was done using Phyre2 (*www.sbg.bio.ic.ac.uk/**phyre2**/) (Kelley and Sternberg, 2009). Structures used were: 3FBV* (Korennykh et al., 2009) *for yIre1 oligomers (Figure 3C), 3P23* (Ali et al., 2011) *for hIre1 face to face dimer (Figure S4A), 2RIO* (Lee et al., 2008) for ADP activated yIre back to back dimer (Figure S4A), *and 3LJO* (Wiseman et al., 2010) *for quercetin activated yIre1 back to back dimer (Figure S4A).*

Cell Culture and IRE1 Foci Microscopy

HEK 293 cells stably transfected with IRE1-GFP (Li et al., 2010) were grown in DMEM media (Cellgro) with 10% FBS and 100 U/ml penicillin, and 100μg/ml streptomycin (Mediatech) in 5% CO_2 at 37°C. To visualize IRE1 foci, cells were grown on a cover slip and the expression of IRE1-GFP was induced upon incubation with 10nM Doxycycline for 24 hrs before start of Thapsigargin (Tg) treatments. Cells were treated with 200nM Tg for up to 8 hrs. Cover slips were then washed with PBS and fixed with 4% PFA. For visualization of IRE1-GFP, cells were then mounted with mounting media containing 1μg/mL DAPI (Pierce) and visualized in the green channel by microscope (Axiovert 200M; Carl Zeiss MicroImaging, Inc.) with a 100X 1.3 NA objective.

Yeast Culture and Northern Blots

Yeast strains used in this study were described in (Chawla et al., 2011); WT (MNY1000), *ire1Δ* (MNY1655), *hac1Δ* (MNY1662). Yeast strains were grown in YPD medium (1% yeast extract, 2% bactopeptone, and 2% glucose) at 30 °C to an OD_{600} of ~0.5 before Tunicamycin (Tm) to a final concentration of 1μg/ml was added and incubated for indicated length of time. At each time point, cells were collected and RNA was isolated for Northern Blot analyses as described previously (Chawla et al., 2011). Briefly, RNA was extracted using the hot phenol method, and RNA was separated on 1.5% agarose gels containing 6.7% formaldehyde and transferred to a Duralon-UV membrane (Agilent Technologies). Splicing of *HAC1* mRNA was examined by hybridization of the membrane with radiolabeled HAC1 probe at 65 °C overnight, and exposed via phosphoimager screen (GE Healthcare). Quantitation was performed using a Typhoon Imager system (GE Healthcare).

Kinase Assay

In vitro Kinase assays were performed as described (Chawla et al., 2011). WT yIre1 or mutant yIre1 proteins were incubated in kinase buffer (10mM Hepes pH 7.5, 5mM $Mg(OAc)_2$, 25mM KOAc, 1mM DTT) with 200 μM of unlabeled ATP and 167 μCi of ^{32}Pγ-ATP (7000Ci/mmol) in a volume of 20μl. Reactions were incubated at 30

°C for 30 min, and hot SDS Loading Buffer and incubation at 95 °C was used to stop the reaction. Samples were immediately run on a 7% SDS-PAGE gel. Phosphorylation was determined by autoradiography and scanned on a Typhoon 9400 (GE Healthcare).

Fractionation of ER

Cells were treated for up to 8 hrs as indicated, washed twice with PBS, and re-suspended in Fractionation Buffer: 10mMHEPES [pH 7.4], 1mM EDTA, 0.25Msucrose, protease inhibitors (Leupeptin, Pepstatin, Aprotinin). Cells were then homogenized by passage through a 27 gage needle and centrifuged at 500Xg for 3min at 4 °C. 150µl of supernatant was then mixed with 2.5M sucrose in Fractionation Buffer, and a flotation gradient was assembled with 1.8M, 1.3M, 0.8M sucrose fractions, with the 1.3M fraction containing the rough microsomes. The gradient was centrifuged at 100,000Xg for 12 hrs, and the 1.3M and 2.5M solutions, corresponding to the ER and cytosolic portions, respectively, were collected. RNA was then extracted using Trizol (Invitrogen) and 10µg of RNA of each fraction was used for Northern Blots as described above.

Oligomerization Assay

Oligomerization assay was done as previously reported (Korennykh et al., 2011). Briefly, reactions were set up using nuclease reaction buffer (40mM Hepes, 7.0, 10mM $Mg(OAc)_2$, 50mM KOAc, 5mM DTT), the indicated amount of WT or mutant yIre1, and 2mM ADP. All reactions were performed in 20µl and incubated for 15 min at 30 °C to allow for oligomerization. The optical density of the sample was measured at 500 nm using a UV-visible spectrophotometer (NanoDrop 2000, Thermo Scientific). Readings were blanked using a reaction without yIre1.

Cell Culture and Determination of XBP1 Splicing and RIDD in vivo

All mammalian cells were cultured in DMEM media (Cellgro) with 10% FBS and 100 U/ml penicillin, and 100ug/ml streptomycin (Mediatech). Cells were grown in 5% CO_2 at 37°C and treated with 200nM Thapsigargin (Calbiochem), 450µM Quercetin (Sigma), or STF-083010 (60µM) (Papandreou et al., 2011) as indicated.

Determination of spliced *XBP1* was performed as described (Lin et al., 2007). Briefly, total RNA was prepared from cells using Trizol (Invitrogen), and 1µg of total RNA was reverse transcribed using Maxima Reverse Transcriptase (Fermentas) to obtain cDNA. cDNA was then PCR amplified using the primers for *XBP1*: 5'-TTACGGGAGAAAACTCACGGC-3' and 5'-GGGTCCAACTTGTCCAGAATGC-3', resulting in a 289 bp fragment corresponding to unspliced *XBP1*, and a 263 bp spliced *XBP1* fragment. Fragments were resolved on a 2.5% agarose gel, and quantified using a Typhoon 9400 fluorescent scanner (GE Healthcare). *XBP1* splicing % was calculated by: [(spliced *XBP1*/(spliced *XBP1*+ unspliced *XBP1*)]X100%.

Determination of RIDD was performed as described (Hollien et al., 2009). Briefly, the same cDNA from

XBP1 splicing assays was used to perform quantitative PCR (qPCR). Reactions were done in triplicate (5ng of input RNA per reaction) for each pair of primers using SYBR Green PCR Master Mix (Applied Biosystems) and 400nM of each primer in a 25μl reaction and analyzed on an ABI Prism 7200 Sequence Detector (Applied Biosystems). Samples were run and quantified using the Standard Curve Method, and expression of each gene was normalized to 18S ribosomal RNA which did not significantly change in any of the conditions. After each run, Melting Curve Analysis was performed to confirm amplification of a single product. Error bars represent standard deviations of the mean calculated from at least three independent experiments. RIDD Activity was calculated by: [(*RIDD* mRNA in untreated cells - *RIDD* in treated cells) / *RIDD* mRNA in untreated cells] X100%. The following primer sets were used for RIDD: *BLOS1* 5'-CAAGGAGCTGCAGGAGAAGA-3' 5'-GCCTGGTTGAAGTTCTCCAC-3'; *SCARA3* 5'-TGCATGGATACTGACCCTGA-3' 5'-GCCGTGTTACCAGCTTCTTC-3' *DAP2*: 5'-GGCTGCGTGGTGGTCAC-3' 5'-CGCATTTCGGGGTATATATCC-3'; *MFα1*: 5'-CGGCTGAAGCTGTCATCG-3'5'-GATACCCCTTCTTCTTTAGCAGCA-3'.

Apoptosis Assays – PARP and Crystal Violet Staining

Construction of cells stably expressing human-yeast chimeric IRE (hyIRE1) containing 1-549aa of hIRE1 and 658-1115aa of yIRE1 was done as described previously (Wiseman et al., 2010). Ire1 knockout MEFs were stably transduced with either hyIRE1 or empty vector and treated with either 200nM thapsigargin (Calbiochem), 450μM Quercetin as described (Wiseman et al., 2010), or 60μM STF-083010 as indicated for up to 48 hrs. RNA was extracted and cDNA was prepared to perform *XBP1* splicing and RIDD activity assays as described above.

Crystal Violet Staining assays were performed in 6 well plates with 2 $X10^5$ cells plated 24hrs before treatment. After treatment, cells were fixed with 10% Formaldehyde; 0.9% NaCl, and stained with Crystal Violet (10% EtOH, 0.05% NaCl, 0.35% Formaldehyde, 0.15% Crystal Violet in 1X PBS). Cells were carefully washed 5 times with 1X PBS, removing excess dye from the plates and leaving only the cells stained. Crystal violet from the cells was then extracted with 2ml 1% SDS in 1X PBS and read by spectrophotometer at an absorbance of 595nm to quantify. The amount of Live Cells (%) (in Figures 4G, S4I, & S4L) was calculated by [(Crystal Violet in untreated cells – Crystal Violet treated cells) / Crystal Violet in untreated cells]X100%.

For analyses of PARP cleavage, cells were collected at each time point and total cell extract was prepared using RIPA buffer (20 mM HEPES (pH 7.4), 150mM NaCl, 1mM EDTA, 1% NP-40, 0.25% NaDeoxycholate, 0.1% SDS, 10mM NaF, 1mM NaVO4, 1mM PMSF, 1mM PMSF, 100u/ml Aprotinin, 1.4 μg/ml Pepstatin, 1μg/ml Leupeptin). Total protein concentrations were normalized by BCA assay (Pierce) and separated on an 8% SDS-PAGE followed by performing western blots using anti-PARP antibody (Cell Signaling) to detect uncleaved PARP and cleaved fragments. PARP Cleavage (%) was calculated using [(cleaved PARP/(uncleaved PARP+ cleaved PARP)]X100%.

SUPPLEMENTAL REFERENCES:

Kelley, L.A., and Sternberg, M.J. (2009). Protein structure prediction on the Web: a case study using the Phyre server. Nature protocols *4*, 363-371.

Niwa, M., Sidrauski, C., Kaufman, R.J., and Walter, P. (1999). A role for presenilin-1 in nuclear accumulation of Ire1 fragments and induction of the mammalian unfolded protein response. Cell *99*, 691-702.

Pettersen, E.F., Goddard, T.D., Huang, C.C., Couch, G.S., Greenblatt, D.M., Meng, E.C., and Ferrin, T.E. (2004). UCSF Chimera--a visualization system for exploratory research and analysis. Journal of computational chemistry *25*, 1605-1612.

Stephens, S.B., Dodd, R.D., Brewer, J.W., Lager, P.J., Keene, J.D., and Nicchitta, C.V. (2005). Stable ribosome binding to the endoplasmic reticulum enables compartment-specific regulation of mRNA translation. Molecular biology of the cell *16*, 5819-5831.